

Research Articles | Behavioral/Cognitive

## Theta-alpha connectivity in the hippocampal-entorhinal circuit predicts working memory load

<https://doi.org/10.1523/JNEUROSCI.0398-23.2023>

Received: 5 March 2023

Revised: 9 November 2023

Accepted: 10 November 2023

Copyright © 2023 the authors

---

*This Early Release article has been peer reviewed and accepted, but has not been through the composition and copyediting processes. The final version may differ slightly in style or formatting and will contain links to any extended data.*

**Alerts:** Sign up at [www.jneurosci.org/alerts](http://www.jneurosci.org/alerts) to receive customized email alerts when the fully formatted version of this article is published.

1 **Theta-alpha connectivity in the hippocampal-entorhinal**  
2 **circuit predicts working memory load**

3 Abbreviated title: Hippocampal-entorhinal circuit supports WM load

4

5 Jin Li (李瑾)<sup>1#</sup>, Dan Cao (曹丹)<sup>2#</sup>, Shan Yu (余山)<sup>2,3</sup>, Haiyan Wang (王海艳)<sup>2</sup>, Lukas  
6 Imbach<sup>4,5</sup>, Lennart Stieglitz<sup>6</sup>, Johannes Sarnthein<sup>5,6\*</sup>, Tianzi Jiang (蒋田仔)<sup>2,3,7\*</sup>

- 7 1. School of Psychology, Capital Normal University, Beijing, 100048, China.  
8 2. Brainnetome Center, Institute of Automation, Chinese Academy of Sciences,  
9 Beijing 100190, China  
10 3. School of Artificial Intelligence, University of Chinese Academy of Sciences,  
11 Beijing 100049, China  
12 4. Swiss Epilepsy Center, Klinik Lengg, Zurich, Switzerland.  
13 5. Zurich Neuroscience Center, ETH and University of Zurich, 8057, Zurich,  
14 Switzerland.  
15 6. Department of Neurosurgery, University Hospital Zurich, University of Zurich,  
16 8091, Zurich, Switzerland.  
17 7. Research Center for Augmented Intelligence, Zhejiang Lab, 311100, Hangzhou,  
18 China.

19 \* **Corresponding author:**

- 20 1. Tianzi Jiang. Email: [jiangtz@nlpr.ia.ac.cn](mailto:jiangtz@nlpr.ia.ac.cn)

21 2. Johannes Sarnthein. Email: johannes.sarnthein@usz.ch

22 # These authors contributed equally.

23

24

25

26 Number of: pages: 50      Number of words: abstract: 162

27                    figures: 6    introduction: 667

28                    tables: 1    discussion: 1201

29                    multimedia: 0

30                    3D models: 0

31

## 32 **Conflict of Interest statement**

33 The authors declare no competing financial interests.

34

## 35 **Acknowledgments**

36 This work received support from the following sources: STI2030-Major Projects

37 (Grant No. 2021ZD0200200 to T.J.), National Natural Science Foundation of China

38 (grant Nos. 32271085 to J.L., 82151307 to T.J.), Strategic Priority Research Program

39 of the Chinese Academy of Sciences (XDB32030207 to T.J.), Open Research Fund of

40 the State Key Laboratory of Cognitive Neuroscience and Learning (CNLYB2004 to  
41 J.L.), and the Swiss National Science Foundation (funded by SNSF 204651 to J.S.).  
42 The authors appreciate the suggestions of Dr. Congying Chu from the Brainnetome  
43 Center in the Institute of Automation, Chinese Academy of Sciences.

44

JNeurosci Accepted Manuscript

## 45 **Abstract**

46 Working memory (WM) maintenance relies on multiple brain regions and inter-  
47 regional communications. The hippocampus and entorhinal cortex (EC) are thought to  
48 support this operation. Besides, EC is the main gateway for information between the  
49 hippocampus and neocortex. However, the circuit-level mechanism of this interaction  
50 during WM maintenance remains unclear in humans. To address these questions, we  
51 recorded the intracranial electroencephalography (iEEG) from the hippocampus and  
52 EC while patients (N=13, 6 females) performed WM tasks. We found that WM  
53 maintenance was accompanied by enhanced theta/alpha band (2-12 Hz) phase  
54 synchronization between the hippocampus to the EC. Granger causality and phase  
55 slope index analyses consistently showed that WM maintenance was associated with  
56 theta/alpha band-coordinated unidirectional influence from the hippocampus to the  
57 EC. Besides, this unidirectional inter-regional communication increased with WM  
58 load and predicted WM load during memory maintenance. These findings  
59 demonstrate that WM maintenance in humans engages the hippocampal-entorhinal  
60 circuit, with the hippocampus influencing the EC in a load-dependent manner.

61

62

63

## 64 **Significance Statement**

65 Hippocampus is known to be part of the working memory (WM) network. How does  
66 the hippocampus communicate with other brain regions to maintain WM information?

67 Rodent studies suggest that hippocampal-entorhinal communication supports WM  
68 maintenance. However, it remains unclear whether and how the human hippocampus  
69 and EC coordinated during WM tasks. In this study, by combining machine learning  
70 analyses with intracranial electroencephalography (iEEG) recordings, we found that  
71 WM maintenance is associated with theta/alpha band (2-12 Hz) unidirectional  
72 influence from the hippocampus to the EC. The unidirectional inter-regional  
73 communication during WM maintenance increased with WM load and predicted WM  
74 load. These findings indicate the hippocampal-entorhinal directional coupling as a  
75 further element of the WM network.

76

77

## 78 **Introduction**

79 Cognition critically depends on the ability to maintain information in an active state  
80 for a short time, which is typically ascribed to working memory (WM)(Baddeley,  
81 2007). Studies found persistent single-neuron spiking (Kaminski et al., 2017;  
82 Kornblith et al., 2017; Boran et al., 2019; Boran et al., 2022) and elevated oscillatory  
83 activity (Li et al., 2022) in the hippocampus during WM maintenance. An increasing  
84 number of studies have pointed out that WM maintenance relies on multiple brain  
85 regions (Christophel et al., 2017) and is supported by inter-regional communication  
86 (Yamashita et al., 2018; Mamashli et al., 2021; Dimakopoulos et al., 2022). Given the  
87 role of hippocampus in WM and the distributed nature of WM, understanding the  
88 connectivity between the hippocampus and the rest of the brain could provide a  
89 crucial insight into the network involved in such a fundamental process. Then, one  
90 may ask how does the hippocampus interact with another/other brain area(s) during  
91 WM maintenance, and which brain area(s) contribute to this process?

92

93 The Entorhinal cortex (EC) is a key candidate to interact with hippocampus for the  
94 following reasons. First, persistent firing during WM maintenance has been  
95 consistently observed in EC neurons across rats (Young et al., 1997), monkeys  
96 (Suzuki et al., 1997) and humans (Boran et al., 2022). Second, the EC serves as an  
97 interface between the hippocampus and cortical/subcortical areas (Lavenex and  
98 Amaral, 2000). Third, structural and functional hippocampal-EC interactions have

99 been extensively reported, involving anatomical connections (Rosene and Van  
100 Hoesen, 1977; Small et al., 2011), sensory information transfer, and memory-  
101 associated activity feedback (Buzsáki and Tingley, 2018; Rozov et al., 2020). Rodent  
102 studies suggest that hippocampal-EC communication supports WM maintenance, as  
103 evidenced by synchronized oscillations during WM execution (Yamamoto et al.,  
104 2014) and WM impairments upon inhibition of this circuit (Suh et al., 2011;  
105 Yamamoto et al., 2014). However, these animal studies have not been validated in  
106 humans, partly due to limitations in noninvasive recording methods' spatial and  
107 temporal resolution. The hippocampal-EC circuit is crucial in spatial navigation  
108 (Zhang et al., 2013), and recent research has extended its involvement to memory-  
109 guided behaviors (Squire, 1992). Building on these findings, our study investigates  
110 the role of this circuit in WM, a fundamental cognitive process with broad  
111 implications (Baddeley, 2012).

112

113 If the hippocampal-EC circuit contributes to WM, understanding the neural  
114 mechanisms underlying this process is crucial. Theta/alpha oscillations (2-12 Hz),  
115 commonly observed in the human medial temporal lobe (Fell et al., 2011; Colgin,  
116 2016), have been implicated in WM. Synchronized oscillations are proposed as a  
117 fundamental mechanism supporting inter-regional neural communication (Fell and  
118 Axmacher, 2011), and low-frequency phase synchronization between the  
119 hippocampus and cortex has been reported during WM maintenance, increasing with



120 WM load (Boran et al., 2019; Dimakopoulos et al., 2022). Granger Causality (GC)  
121 and phase slope index (PSI) are popular techniques used to estimate the directionality  
122 of inter-regional interactions. Previous research has reported the role of theta/alpha-  
123 gamma phase-amplitude coupling (PAC) in WM maintenance (Roux and Uhlhaas,  
124 2014). However, most studies have focused on PAC within a single brain region, like  
125 the hippocampus (Axmacher et al., 2010), with limited inter-regional exploration  
126 (Wang et al., 2021). Theta-gamma interactions have been observed in hippocampal-  
127 EC communication in rodent studies (Buzsáki, 2002; Hasselmo et al., 2002). The  
128 involvement of inter-regional low-frequency synchronization and cross-frequency  
129 coupling in the hippocampal-EC circuit during WM processing remains unclear.

130

131 Leveraging the high spatiotemporal resolution of iEEG recordings and the analytical  
132 power of multivariate machine-learning analysis, we tested the hypothesis that low  
133 frequency and gamma oscillations cooperatively facilitate hippocampal-EC  
134 interactions to support the maintenance of WM information in humans. We  
135 simultaneously recorded iEEG data from the hippocampus and EC in 13 epilepsy  
136 patients while they performed a modified Sternberg task (Michels et al., 2008; Boran  
137 et al., 2019; Li et al., 2022). Our goal was to address the following questions: (a) Do  
138 the hippocampus and the EC interact while humans perform a WM task? (b) Which  
139 specific oscillatory modes of interregional communication, including frequency and

140 directionality, mediate WM maintenance? And (c) Do these interaction modes have  
141 functional effects?

142

## 143 **Materials and methods**

### 144 **Participants**

145 We used data from 13 adult human patients (mean  $\pm$  SD [range]: 35 $\pm$ 13 [18-56]; 6  
146 females) in this study. All patients were implanted with depth electrodes (1.3 mm  
147 diameter, 8 contacts of 1.6 mm length, and 5 mm spacing between contact centers;  
148 Ad-Tech, Racine, WI, [www.adtechmedical.com](http://www.adtechmedical.com)) in the medial temporal lobe for  
149 evaluation of the surgical treatment of epilepsy. Electrode placement was exclusively  
150 guided by clinical needs. There were no seizures recorded during any of the recording  
151 sessions, and any trials with interictal epileptiform activity were excluded from  
152 analysis. All patients provided written informed consent before participating. This  
153 study has been approved by the relevant institutional ethics review board (Kantonale  
154 Ethikkommission Zürich, PB 2016-02055), and is in agreement with the Declaration  
155 of Helsinki.

### 156 **Experimental design**

157 We used a modified Sternberg task in which the encoding of memory contents, their  
158 maintenance, and their recall were temporally separated (**Fig. 1A**). Each trial started

159 with a fixation period (1 s) followed by the stimulus for 2 s. Participants were  
160 instructed to memorize a set of four, six, or eight letters that were presented at the  
161 center of the screen. The number of letters indicated the memory load. After the  
162 disappearance of the stimulus, the maintenance interval followed (3 s). After  
163 presentation of the probe letter, the participants responded with a button press (“IN”  
164 or “OUT”) to indicate whether the probe was part of the stimulus letter set. After the  
165 response, the participants were encouraged to relax before they initiated the next trial.  
166 The participants performed 50 trials per session, which lasted approximately 10 min.  
167 During the recording period of several days, several participants performed more than  
168 one session of the task up to a total of eight sessions. **Table 1** contains detailed  
169 information about the number of trials and sessions for each participant. To eliminate  
170 any potential confusion arising from mixing categories with varying proportions of  
171 incorrect trials, subsequent analyses exclusively utilized trials with correct responses.

## 172 **Channel localization and selection**

173 Channel localization was performed using postimplantation computed tomography  
174 (CT) scans and structural T1-weighted MRI scans. For each patient, the CT scan was  
175 co-registered to the postimplantation scan, as implemented in the FieldTrip toolbox  
176 (Oostenveld et al., 2011). The channels were visually marked on the coregistered CT-  
177 MR images. The channel positions were then normalized to the MNI 152 space and  
178 assigned to specific brain regions using the Brainnetome Atlas (Fan et al., 2016).  
179 Channel positions were verified by the neurosurgeon (L.S.) after merging pre-

180 operative MRI with postimplantation CT images of each individual patient in the  
181 plane along the electrode (iPlan Stereotaxy 3.0, Brainlab, München, Germany).

182

183 For each participant we analyzed the iEEG from a maximum of three electrodes per  
184 hemisphere targeting the hippocampal head (anterior), the hippocampal body  
185 (posterior), and the entorhinal cortex. Targeted regions and hemispheres varied across  
186 participants for clinical reasons and included the hippocampus in the left ( $n = 12$ ) and  
187 right ( $n = 13$ ) hemisphere and the entorhinal cortex in the left ( $n = 12$ ) and right ( $n =$   
188 11) hemisphere. We selected the two most medial channels on each electrode  
189 targeting the hippocampus or the entorhinal cortex as in previous studies (Oehrns et al.,  
190 2014; Pacheco Estefan et al., 2019). The final number of selected channels in each  
191 region for each participant is listed in **Table 1**. We included only ipsilateral channel  
192 pairs in the analysis. The final dataset contained 87 channels in the hippocampus and  
193 46 channels in the entorhinal cortex across all patients. There were  $6.7 \pm 1.5$  (range 4-  
194 8) channels per patient in the hippocampus and  $3.5 \pm 0.9$  (range 2-4) channels per  
195 participant in the entorhinal cortex. **Fig.1C** presents all recording locations with the  
196 BrainNet Viewer toolbox (Xia et al., 2013) in MATLAB (MathWorks, Natick, MA).

### 197 **Data acquisition and preprocessing**

198 Intracranial data were acquired using a Neuralynx ATLAS recording system, sampled  
199 at 4 kHz, and analog-filtered above 0.5 Hz. The data were recorded against a common  
200 reference where the outermost electrode contact in temporal cortex served as

201 electrical reference. After data acquisition, neural recordings were downsampled to 1  
202 kHz and band-pass filtered from 1 to 200 Hz using the zero-phase delay finite impulse  
203 response (FIR) filter with a Hamming window. Line noise harmonics were removed  
204 using a discrete Fourier transform. The filtered data were manually inspected to mark  
205 any contacts or epochs containing epileptiform activity or artifacts for exclusion and  
206 were then re-referenced. The continuous data were segmented into 8 s trials with a 1 s  
207 fixation period as the baseline, 2 s encoding period, 3 s maintenance period, and 2 s  
208 retrieval period. We here focused on the maintenance period. The trials with residual  
209 artifacts were rejected after visual inspection. In total, we rejected 65 trials with load 4  
210 (5.5%), 36 trials with load 6 (3.9%) and 39 trials with load 8 (5.1%) across all  
211 participants. Preprocessing routines were performed using the FieldTrip toolbox  
212 (Oostenveld et al., 2011) and customized scripts in MATLAB.

### 213 **Statistical analyses**

214 To assess the significance of a value, we created a null distribution estimated from  
215 1000 permutations on data with scrambled labels using a non-parametric permutation  
216 test. The significance was defined as exceeding the threshold that obtained from the  
217 95<sup>th</sup> percentile of the empirically estimated null distribution.

218

219 To compare the metrics of phase synchronization, GC, PAC and PSI between two  
220 loads (load 4 vs load 6, load 4 vs load 8, load 6 vs load 8), the statistical significance  
221 was then estimated using a permutation test, in which a null distribution was created  
222 by randomly assigning trials into two loads, computing the differences between loads,

223 and repeating this procedure 1000 times. We also applied paired *t*-tests to directly  
224 compared measurements from the two directions within each load condition. Multiple  
225 comparisons were corrected by False Discovery Rate (FDR).  $P < 0.05$  was considered  
226 significant.

227

228 To rule out potential confounding effects of aperiodic activity on WM load, we first  
229 performed separate repeated-measures analyses of variance (ANOVAs) for the  
230 hippocampus and the EC, with a within-group effect of load across the frequency  
231 spectrum. The aperiodic activity was chosen as it captures non-oscillatory effects at  
232 specific frequency, allowing us to examine the precise frequency ranges sensitive to  
233 load effect on non-oscillatory components. Additionally, we applied a linear-mixed  
234 effect model to explore whether the aperiodic activity from the hippocampus and the  
235 EC contributed to the hippocampus-EC interaction, with load, the aperiodic activity as  
236 fixed factors, and participants as a random factor, and the electrophysiological  
237 indexes as dependent variables.

238

239 For all the decoding analyses, we used a non-parametric permutation approach to test  
240 the significance of the accuracy values. We created a null distribution of the decoding  
241 accuracy by shuffling the data labels 1000 times. For each decoding analysis, the null  
242 distribution was generated for each test and we took the maximum value of the null  
243 distributions across tests as a final null distribution for multiple corrections, as  
244 previous study did (Mamashli et al., 2021). The averaged decoding accuracy  
245 exceeding the 95<sup>th</sup> percentile of such null distribution ( $p < 0.05$ ) was considered  
246 significant.

247 **Time-frequency analysis**

248 Time-frequency power was separately computed within the hippocampus and the EC  
249 for trials with different WM loads. For each trial and each channel, we convolved the  
250 signal with complex-valued Morlet wavelets (6 cycles) to obtain power information at  
251 each frequency from 1 to 100 Hz (in steps of 1 Hz) with a time resolution of 1 ms.  
252 The task-induced power was analyzed per trial using a statistical bootstrapping  
253 procedure (methods have been described in more detail in our previous publication  
254 (Li et al., 2022)). Then, the raw power for each time point during the task was  $z$ -  
255 scored by comparing it to the null distribution to generate the  $z$ -scored power. For  
256 each participant, the  $z$ -scored spectral power in the theta/alpha band was averaged  
257 across the maintenance period within the hippocampus and the EC separately for each  
258 WM load.

259

260 Previous study reported that periodic properties of electrophysiological data are  
261 highly variable, and also coexist with variable and dynamic aperiodic activity  
262 (Donoghue et al., 2020a; Donoghue et al., 2020b; Donoghue and Watrous, 2023). To  
263 exclude possible confounding effect of aperiodic activity on neural oscillations of the  
264 hippocampus and EC, we have adopted a distinct approach by separately  
265 characterizing the aperiodic properties of power spectra originating from both the  
266 hippocampus and the EC, with the Fitting-Oscillations-and-One-Over-F (FOOOF)  
267 toolbox (Donoghue et al., 2020b). We isolated the aperiodic component of power  
268 spectra across the entire frequency spectrum for each load and region, and compared

269 these components among WM load for each region with the repeated-measures  
270 ANOVA.

### 271 **Phase-locking value**

272 To explore the potential interaction between the hippocampus and the EC during WM  
273 maintenance, we employed phase-locking value (PLV) to assess the degree of  
274 consistency for each channel pair phase relationship independent of their absolute  
275 phases and amplitudes among repeated trials, with  $PLV = 1$  referring to strong phase  
276 synchrony where all trials are synchronized without any variations between two  
277 channels. Using the same parameters of time-frequency analysis, we computed the  
278 PLV in the time-frequency domain from 1-100 Hz during maintenance for each  
279 channel pair within the same hemisphere (one channel from the hippocampus and one  
280 from the EC) for the trials with each WM load.

281

282 To evaluate the statistical significance of PLV, a null distribution was created by  
283 randomly shuffling the trials with load8 for each channel pair and computing the  
284 corresponding PLV spectrogram and repeating the same procedure for 1000 times, as  
285 our previous study did (Boran et al., 2019). Then the null distribution of all channel  
286 pairs was averaged and only the time-frequency PLV above the threshold (95% of the  
287 null distribution) were kept as significant PLV for further analyses. In addition, the  
288 workload-dependent increases in the PLV were subsequently assessed by subtracting



289 the PLV for trials with one load from the PLV for another load, and the statistical  
290 significance between two loads was then estimated using a permutation test, as  
291 mentioned in the section of statistical analyses.

## 292 **Granger Causality analysis**

293 After establishing the phase synchrony, which measures undirected connectivity  
294 between the hippocampus and EC, we proceeded to investigate the directionality of  
295 their interaction using two complementary measures: a frequency-domain GC and  
296 PSI. GC measures the degree to which the signal from a region (i.e., the  
297 hippocampus) can be better predicted by incorporating information from another  
298 signal (i.e., the EC) in a specific frequency band, and vice versa (Zheng et al., 2019).  
299 For each channel pair, the trial-wise mean was subtracted from each trial before fitting  
300 to an autoregressive model and computing the spectral GC. We then used the  
301 Multivariate Granger Causality Matlab Toolbox (Barnett and Seth, 2014) based on the  
302 Akaike information criterion to define the model order for each pair. Based on the  
303 observations from the PLV above, we computed the GC index across 2-12 Hz (in  
304 steps of 0.25 Hz) for both directions (from the hippocampus to the EC and the reverse  
305 direction) with the trials of load 4, load 6 and load 8, separately. To test the statistical  
306 significance of GC, we created a null distribution by randomly shuffling the signal  
307 between the channel pairs 1000 times and averaged the null distribution of all channel  
308 pairs. Only the value above the threshold (95% of the null distribution) was kept as  
309 significant GC for further analyses. For the GC index across 2-12 Hz from the

310 hippocampus to the EC as well as the opposite direction, we also applied the  
311 permutation test for comparisons between two loads, as mentioned in statistical  
312 analyses. To rule out the bias of aperiodic activity, with the linear mixed-effect model,  
313 we considered WM load, the aperiodic activity of the hippocampus and the EC within  
314 2-12 Hz as fixed factors, and the participants as a random factor. The hippocampal  
315 driven GC as well as the EC driven GC across 2-12Hz was set as the dependent  
316 variable.

### 317 **Phase slope index analysis**

318 On the other hand, PSI examines whether the slope of the phase differences between  
319 the channel pairs remains consistent across several adjacent frequency bins (Nolte et  
320 al., 2008). A positive PSI signifies that the channel in the first structure (e.g.,  
321 hippocampus) leads the channel in the second structure (e.g., EC), whereas a negative  
322 PSI indicates the reverse. For the trials with WM load, using the FieldTrip toolbox  
323 (Oostenveld et al., 2011), the data segments during maintenance were zero padded  
324 and multiplied with a Hann taper from 2 to 12 Hz with 1 Hz step, from which we  
325 computed the theta/alpha PSI at each channel pair within the same hemisphere in each  
326 participant (i.e., one from the hippocampus and the other from the EC) and pooled all  
327 possible channel pairs between the hippocampus and EC for each participant. To  
328 correct for any spurious results, we randomly shuffled the trials and recomputed the  
329 PSI at each channel pair. This step was repeated 1000 times to create normal  
330 distributions of channel pair-resolved null PSI data.

331

332 To construct a directional effect of the hippocampus-EC on a population level, we  
333 averaged the raw PSI across channel pairs and participants. Correspondingly, the null  
334 distributions were also averaged across channel pairs and participants. Consequently,  
335 the raw PSI outputs can be compared to the distribution of null PSI to derive a  $z$ -score  
336 in the theta/alpha band (for a similar approach, see (Solomon et al., 2019)). To  
337 examine if the null distribution of PSI by randomization is a normal distribution, we  
338 assessed the normality of the null distribution for different WM loads using the  
339 Jarque-Bera test, a widely used statistical test that examines the skewness and kurtosis  
340 of a sample to determine its normality. The null distribution of PSI for load4, load6,  
341 and load8 is normally distributed (Jarque-Bera test: load4,  $p = 0.13$ ; load6,  $p = 0.11$ ;  
342 load8,  $p = 0.50$ ). As a result, raw PSI outputs were  $z$ -scored and significant PSI was  
343 thresholded at  $|z| > 1.96$ , in which the hippocampus leads were defined as  $z > 1.96$  and  
344 the EC leads as  $z < -1.96$  as in our previous study (Li et al., 2022; Li et al., 2023b).

345

346 To assess the statistical significance of PSI differentiation for WM load, the  
347 permutation test described previously was also used here to create a null distribution  
348 of PSI differences between two loads. Then the real PSI differences were obtained  
349 between loads and were then compared with the corresponding null distribution to  
350 estimate a  $z$ -score with the positive value indicating PSI increase in the high load  
351 condition versus the low load condition.

### 352 **Cross-regional phase-amplitude coupling**

353 Next, we investigated the cross-regional PAC between the hippocampus and the EC  
354 using the modulation index (MI) (Tort et al., 2010; Vaz et al., 2017), which reflects

355 the coordinated activity between brain regions. We first calculated the time series of  
356 phase and amplitude envelope. This was achieved by applying the standard Hilbert  
357 transform to the low-frequency (2-30 Hz) phase, extracted from the hippocampus/EC  
358 channel, using a 2 Hz step. Similarly, the high-frequency (30-150 Hz) amplitude was  
359 obtained from the channel in the other structure (EC/hippocampus) with a 5 Hz step.  
360 Subsequently, we partitioned the continuous phase values of the modulating  
361 frequency into 20 evenly spaced phase bins. For each phase of the low-frequency  
362 modulating signal, we determined the corresponding amplitude of the high-frequency  
363 modulated signal and assigned it to the respective phase bin. To assess this coupling,  
364 we employed the MI that quantifies the disparity in entropy between the computed  
365 phase-amplitude distribution and a uniform distribution using a normalized Kullback-  
366 Leibler distance between each pair of low modulating frequencies and high modulated  
367 frequencies.

368

369 To assess the statistical significance of PAC, we generated a null distribution with a  
370 trial shuffling procedure. Specifically, we created shuffled versions by associating the  
371 phase series of trial  $k$  with the amplitude series of trial  $l$ , with  $k$  and  $l$  randomly chosen  
372 among the trial numbers. We then generated 1000 surrogate MI values, from which  
373 we could infer the MI chance distribution. To construct a directional effect of PAC on  
374 a population level, we averaged the raw PAC across channel pairs and participants.  
375 Correspondingly, the null distributions were also averaged across channel pairs and

376 participants. Consequently, the raw PAC outputs can be compared to the distribution  
377 of null PAC to derive a  $z$ -score in the phase and amplitude frequency band.  
378 Significant zPAC was thresholded at  $|z| > 1.96$ .

379

380 We also examined the relationship between cross-regional theta/alpha-gamma zPAC  
381 and WM load with the permutation tests for comparisons between two loads.

382 Thresholding was performed at the 95<sup>th</sup> percentile level, as stated in the statistical  
383 analyses section. Similarly, as done in Granger causality analysis, the linear mixed-  
384 effect model was applied to examine the effect of the aperiodic activity on zPAC.

385 Specifically, we treated WM load, the aperiodic activity of the hippocampus (2-12  
386 Hz) and of the EC (30-100 Hz) as fixed factors, and the participants as a random  
387 factor. The hippocampal theta/alpha phase - EC gamma amplitude zPAC as well as  
388 the opposite direction were set as the dependent variables. We also tested the impact  
389 of phase synchrony to the functional effect of zPAC within the same model, as  
390 previous study conducted (Wang et al., 2021).

### 391 **Machine learning analyses**

392 In addition to conventional univariate analysis, multivariate analysis detects subtle  
393 load-related distribution pattern changes missed by univariate methods (Grootswagers  
394 et al., 2017), and enhances findings' generalizability and reliability through inter-  
395 subject validation (Wang et al., 2020). Therefore, we next investigated whether the

396 neural activity and inter-regional communication within the hippocampal-EC circuit  
397 was modulated by WM load. We used the patterns from PLV, GC, zPAC, and z-  
398 scored power from the trials with WM load as our features. Here we used support  
399 vector machine (SVM) (Chang and Lin, 2011) as a classifier to classify the WM load  
400 (load 4/6/8). SVM is widely used in decoding analyses in neuroimaging studies  
401 (Mamashli et al., 2021) because of its suitability for analyses with a relatively small  
402 number of samples. It is provided by the COSMOMVPA package (Oosterhof et al.,  
403 2016) in MATLAB. And the approach of leave-one-out cross-validation (LOOCV)  
404 was applied to validate the decoding accuracy. Considering the inherent difficulty of  
405 generalizing across different subjects (Poldrack et al., 2009; Poldrack, 2011), leave-  
406 one-out cross-validation (LOOCV) is shown to be a suitable method for obtaining  
407 dependable accuracy estimates, especially when working with datasets that have a  
408 restricted number of samples (Wong, 2015). Details of our multivariate pattern  
409 analysis (MVPA) decoding analyses were as follows:

410 (A) PLV patterns: We considered the theta/alpha (2-12 Hz) PLV patterns between the  
411 hippocampus and the EC during maintenance to investigate whether the phase  
412 synchrony pattern could decode the WM load. For each participant and each load,  
413 there were  $M$  features (11 frequency bins  $\times$  3000 time bins) converted to a feature  
414 vector. We trained a linear SVM classifier and applied LOOCV at subject level by  
415 splitting the data set of all subjects ( $N = 14$ ) into a training set from  $N-1$  subjects and  
416 a testing set from the remaining one subject. This process was repeated  $N$  times to

417 ensure comprehensive validation. For each iteration, we used the feature vectors  
418 labeled as load 4, load 6 and load 8 from the training dataset, which encompassed the  
419 data of  $N-1$  participants. This resulted in a training dataset including  $(N-1)$   
420 participants  $\times$  3 sets  $\times$   $M$  features. Subsequently, we calculated the average  
421 classification accuracy by averaging the results across the  $N$  repetitions of the cross-  
422 validation procedure. Meanwhile, to reduce the feature dimensionality, principal  
423 component analysis (PCA) was applied to the training data set to keep several  
424 principal components ( $K$  components) that explained 99% of the variance in the data.  
425 We also applied the  $K$  components matrix on the remaining data set from one  
426 participant and tested the SVM classifier. This procedure was replicated  $N$  times for  
427 cross-validation. The schematic of the MVPA using the feature patterns is shown in  
428 **Fig. 1D**. The accuracy of the classifier was averaged across  $N$  cross-validations as a  
429 measure of performance. To test the significance of the accuracy, we created a null  
430 distribution by shuffling the training labels 1000 times. And the averaged decoding  
431 accuracy exceeding the 95<sup>th</sup> percentile of the null distribution ( $p < 0.05$ ) was  
432 considered significant.

433 (B) GC patterns: We considered the GC patterns from two directions, from the  
434 hippocampus to the EC and the reverse direction, to allow us to investigate whether  
435 there was a specific information flow pattern that could decode the WM load. The GC  
436 patterns were calculated in the theta/alpha band separately for trials with different  
437 WM load. For each participant and each load, the GC pattern included  $M$  values ( $M =$   
438 41) and these values were converted into a feature vector. As described above, we

439 used the feature vectors labeled as load 4, load 6 and load 8 from  $N-1$  participants as a  
440 training data set ( $N-1 \times 3$  sets  $\times M$  features) and tested these on the remaining one  
441 participant data set. Similar to the LOOCV performed in the previous analysis, we left  
442 one participant out for validation and replicated this procedure  $N$  times. The accuracy  
443 of the classifier was averaged across all replications. In total, we separately performed  
444 this classification process for the 2 directions: for the hippocampus modulating the EC  
445 and for the EC modulating the hippocampus. Similar to the PLV patterns, we  
446 generated a null distribution with each direction of GC patterns and took the  
447 maximum value of the two null distributions as the final null distribution for multiple  
448 corrections, as previous study did (Mamashli et al., 2021). The averaged decoding  
449 accuracy exceeding the 95<sup>th</sup> percentile of the null distribution ( $p < 0.05$ ) was  
450 considered significant.

451 (C) Z-scored PAC patterns: We calculated the theta/alpha phase-gamma band zPAC  
452 between the hippocampus phase modulating the EC amplitude and the opposite  
453 direction differences for the trials of load 4, load 6 and load 8 separately. For each  
454 participant and each load, there were  $M$  features (11 phase bins  $\times$  36 amplitude bins)  
455 converted to a feature vector. Similar as described for the PLV patterns, we combined  
456  $N-1$  participants' data set from trials with WM load as training data set, applied zPCA  
457 to the training data set to  $K$  components that explained 99% of the variance, fed the  
458 features ( $N-1 \times 3$  sets  $\times K$  components) into a linear SVM classifier and trained the  
459 classifier, and tested it on the remaining one participant data set that already applied  $K$   
460 components matrix to the testing data set. The accuracy of the classifier was averaged  
461 across  $N$  replications. To test the significance of the accuracy, we created a null  
462 distribution by shuffling the training labels 1000 times. And the averaged decoding



463 accuracy exceeding the 95<sup>th</sup> percentile of the null distribution ( $p < 0.05$ ) was  
464 considered significant.

465 (D) *Z*-scored power patterns: To address whether local activity in the hippocampus  
466 and the EC contributed to WM load, we used a frequency specific *z*-scored power  
467 pattern at the theta/alpha band (2-12 Hz, 11 frequency bins) during maintenance from  
468 the hippocampus and EC to decode the WM load. The training data set for the linear  
469 SVM classifier from  $N-1$  participants ( $N-1 \times 3$  sets  $\times M$  features) and the classifier  
470 was tested on the remaining one participant data set. The accuracy of the classifier  
471 was averaged across  $N$  replications by LOOCV. We performed 2 classifications (2  
472 regions) in this decoding analysis and the statistical analysis was performed aligns  
473 with the above analyses.

474

## 475 **Results**

### 476 **Task, behavior and recording channels**

477 Thirteen patients with drug resistant epilepsy (6 female) performed a modified  
478 Sternberg WM task during an invasive presurgical evaluation. In this task, the items  
479 were presented simultaneously rather than sequentially, thus separating the encoding  
480 period from the maintenance period. In each trial, the participant was asked to  
481 memorize a set of four, six, eight letters presented for 2 s (encoding). The number of  
482 letters was thus specific for the memory load (load4, load6 and load8). After a delay  
483 (maintenance) period of 3 s, a probe letter was presented and the participant

484 responded whether the probe letter was identical to one of the letters held in memory  
485 (retrieval) (**Fig. 1A**). Across all sessions, participants' averaged capacity was 7.2,  
486 calculated by Cowan's formula (Cowan, 2001), which indicated that the participants  
487 were able to maintain about 7 letters in memory. The response accuracy of the  
488 participants decreased from load4 (mean  $\pm$  S.D.: 97.89%  $\pm$  1.90%) to load6  
489 (91.03%  $\pm$  5.49%) and to load8 (85.49%  $\pm$  6.11%) (repeated-measures analysis  
490 of variance (ANOVA),  $F(2,24) = 36.55$ ,  $p < 0.001$ , **Fig. 1B**). This finding indicates that  
491 the behavioral performance of participants was modulated by WM load. The response  
492 accuracy for each participant is listed in **Table 1**. We recorded local field potentials  
493 from depth electrodes implanted in the hippocampus and the EC (**Fig. 1C**) while  
494 participants performed the task. Across all participants, 87 channels in the  
495 hippocampus and 46 channels in the EC were included in the subsequent analysis (see  
496 the details in **Methods**).

#### 497 **Theta/alpha synchronization in the hippocampal-entorhinal circuit as a function** 498 **of WM load**

499 To explore the potential interaction between the hippocampus and the EC during WM  
500 maintenance, we employed phase locking values (PLVs) to assess the coherence of  
501 phase relationships among each channel pair connecting the two regions. The PLV up  
502 to 100 Hz was computed in the time-frequency domain to reveal the dynamic  
503 fluctuations of the functional connectivity. As shown in **Fig.2A**, the phase  
504 synchronization up to 12 Hz (permutation test,  $p < 0.05$ ) was found significantly

505 between the hippocampus and the EC throughout the entire maintenance period  
506 regardless of WM load. And this finding was confirmed by the spectral PLV across  
507 the time domain, which the real phase synchronization of hippocampal-EC was  
508 existed in the theta/alpha band (2-12 Hz; **Fig.2B**, gray area) that exceeded the  
509 threshold from the permutation test on the PLV with trials of load8 (**Fig.2B**, black  
510 line). To examine whether the theta/alpha PLV was increased with WM load increase,  
511 we made a cluster-based permutation test on the theta/alpha PLV between two load  
512 conditions for the time-frequency space across participants. As presented in **Fig.2C**,  
513 the theta/alpha PLV in the high load condition (load6/8) was higher relative to the low  
514 load condition (load4) during maintenance (cluster-based permutation,  $p < 0.05$ ),  
515 which demonstrated consistent frequency effects during maintenance. To confirm  
516 whether the theta/alpha PLV was modulated by WM load, we separately calculated  
517 the theta/alpha PLV for load 4, load 6 and load 8 and compared the PLV between  
518 loads using a permutation test with FDR correction. Results also indicated that the  
519 theta/alpha PLV was larger in the higher load conditions than in load4 (FDR  
520 corrected: load4 vs load6,  $p = 0.0042$ ; load4 vs load8,  $p = 0.006$ ; load6 vs load8,  $p =$   
521  $0.15$ ; **Fig.2D**).

522

523 Next, we investigated whether inter-regional phase synchronization predicts WM  
524 load. Support vector machine (SVM) classifiers show good generalization  
525 performance for high dimensional data and have been widely used for classifying

526 scalp EEGs (Kumar and Gupta, 2021) and have recently been successfully used for  
527 classifying magnetoencephalography signals (Mamashli et al., 2021). Hence, we used  
528 a linear SVM classifier here to decode WM load (load 4, load 6 or load 8) on the  
529 participant level with theta/alpha PLV as features (**Fig. 1D**). Previous studies  
530 suggested that leave-one-out cross-validation (LOOCV) is applicable to obtain a  
531 reliable accuracy estimate for a classification algorithm when the number of sample in  
532 a data set is small (Wong, 2015). Thus, we applied LOOCV by splitting the data set of  
533 all participants ( $N = 13$ ) from WM load into a training set of  $N-1$  participants and a  
534 testing set of the remaining one participant, and then replicated this procedure by  $N$   
535 times. An average decoding accuracy was obtained across all cross-validations ( $N$   
536 times) for the classification of WM load. The statistical significance of the  
537 classification accuracy was determined by comparing the original accuracy with a null  
538 distribution created by using a randomized classifier by permuting the labels 1000  
539 times (see details in **Methods**). As shown in **Fig.2E**, decoding accuracy using the  
540 theta/alpha PLV features for WM load ( $41.03\% \pm 4.05\%$ ) was significantly above  
541 chance level (permutation test against scrambled labels,  $p < 0.05$ ). These results  
542 suggest that the theta/alpha PLV between the hippocampus and the EC can predict  
543 WM load for individual participants.

544 **Directional information transfer from the hippocampus to the EC carries**

545 **information on WM load**

546 To further examine the functional relevance of directionality in the hippocampal-EC  
547 synchronization, we applied a frequency-domain GC analysis to quantify the inter-  
548 regional directional influence. We separately computed the spectral GC index in the  
549 theta/alpha band for trials with load4, load6 and load8 between the hippocampus and  
550 the EC during maintenance. Then, we examined the association between WM load  
551 and the information flow from the hippocampus to the EC and from the opposite  
552 direction, separately, using the permutation test with FDR correction. As presented in  
553 **Fig. 3A**, the GC index from the hippocampus was larger in load8 condition than in  
554 load4 (FDR corrected: load4 vs load6,  $p = 0.056$ ; load4 vs load8,  $p = 0.012$ ; load6 vs  
555 load8,  $p = 0.30$ ). While there was no load effect on information transfer for the  
556 opposite direction (all  $ps > 0.05$ ). Moreover, no significant differences in information  
557 flow between the hippocampus and EC were observed for all load conditions (paired  
558  $t$ -tests, all  $ps > 0.05$ ).

559

560 We next investigated whether the directional information flow between the  
561 hippocampus and the EC could predict WM load. The GC index in the theta/alpha  
562 band from both directions were calculated as features to decode the WM load. As  
563 shown in **Fig. 3B**, WM load could be decoded by using the GC features from the  
564 hippocampus to the EC ( $43.59\% \pm 5.83\%$ ; permutation test against scrambled labels,

565  $p < 0.05$ ) but not in the opposite direction ( $41.03\% \pm 5.54\%$ ;  $p > 0.05$ ). These results  
566 provide evidence at the level of individual participants that WM load affected the  
567 theta/alpha directional information transfer from the hippocampus to the EC.

568

569 Given that the GC analysis is sensitive to the signal-to-noise ratio across frequency  
570 bands (Cohen, 2014), we confirmed the directionality between the hippocampus and  
571 the EC by calculating the phase slope index (PSI) (Nolte et al., 2008) in the  
572 theta/alpha band (2-12 Hz). **Fig.3C** presents the  $z$ -scored PSI in the theta/alpha band  
573 for the load 4, load 6 and load 8 conditions. The  $z$ -scored PSI differed between the  
574 low (load4) and high loads (load6/load8). In particular, the hippocampus-driven  
575 information flow was larger in load6 and load8 than the load4 condition (permutation  
576 test: load4 vs load6,  $z = 2.29$ ,  $p = 0.022$ ; load4 vs load8,  $z = 3.02$ ,  $p = 0.0025$ ; FDR  
577 corrected). These results confirm the findings from the GC analysis. Together they  
578 indicate that the hippocampus-driven information transfer carries the information of  
579 WM load.

### 580 **Cross-regional phase-amplitude coupling within the hippocampal-entorhinal** 581 **circuit predicts WM load**

582 Cross-regional PAC serves as a mechanism for organizing brain activity across  
583 regions. Therefore, we performed cross-regional PAC in both phase-amplitude  
584 combinations (low-frequency phase from the hippocampus and high-frequency

585 amplitude from the EC, and vice versa) using a modulation index (MI) (Tort et al.,  
586 2010; Vaz et al., 2017). To remove PAC expected by chance, the raw PAC was  $z$ -  
587 scored against surrogate distributions across channel pairs and participants on a  
588 population level (see Methods for details), as previous studies did (Solomon et al.,  
589 2019). As presented in **Fig.4A**, there was evident  $z$ PAC ( $|z| > 1.96$ ) between the  
590 theta/alpha phase of the hippocampus and the gamma amplitude of the EC for each  
591 load, while no significant coupling was found in the opposite direction ( $|z| < 1.96$ ,  
592 **Fig.4B**). Thus, we extracted hippocampal theta/alpha phase – EC gamma amplitude  
593  $z$ PAC for further analyses.

594

595 To examine the association between cross-regional  $z$ PAC and WM load, we compared  
596 theta/alpha-gamma  $z$ PAC under different load conditions. Results showed stronger  
597 hippocampal theta/alpha phase – EC gamma amplitude  $z$ PAC in the high load  
598 condition (load6/8) compared to load4 (permutation test: load4 vs load6,  $p = 0.047$ ;  
599 load4 vs load8,  $p = 0.046$ ; load6 vs load8,  $p = 0.61$ ; **Fig.4C**). Given the significant  
600 theta/alpha PLV findings, we added theta/alpha PLV as a regressor to examine  
601 whether it contributed to the functional effect of hippocampal theta/alpha phase – EC  
602 gamma amplitude  $z$ PAC, as previous study did (Wang et al., 2021). Our analyses  
603 revealed that the effect of WM load on  $z$ PAC was still significant (linear mixed-  
604 effects model:  $p = 0.011$ ,  $t = 2.71$ ), when controlling for the PLV ( $p = 0.16$ ). Our

605 findings indicated that the load effect on hippocampal theta/alpha phase – EC gamma  
606 amplitude  $z$ PAC could not be explained by PLV differences.

607

608 Additionally, we fed the hippocampal theta/alpha phase – EC gamma amplitude  $z$ PAC  
609 features into the linear SVM classifier to decode the WM load. We found that the  
610 decoding accuracy using cross-regional  $z$ PAC with the theta/alpha phase of the  
611 hippocampus modulating the gamma amplitude of the EC reached a significant level  
612 ( $51.28\% \pm 8.12\%$ ; permutation test against scrambled labels,  $p < 0.05$ , **Fig.4D**). These  
613 results are in line with the univariate analysis.

#### 614 **Effect of WM load on inter-regional interaction between the hippocampal** 615 **subregion and EC**

616 The hippocampus, a complex structure, comprises anterior and posterior subregions  
617 that exhibit distinct function during WM maintenance (Li et al., 2022). Consequently,  
618 we performed separate analyses for the anterior hippocampus-EC and posterior  
619 hippocampus-EC connections. Utilizing permutation tests with FDR correction, we  
620 compared the metrics of PLV, GC, and PAC between different WM loads. Regarding  
621 the theta/alpha PLV between the anterior hippocampus and the EC, we found a  
622 significantly higher PLV in load 8 compared to load 4/6 (FDR corrected: load4 vs  
623 load8,  $p = 0.036$ ; load6 vs load8,  $p = 0.045$ ; **Fig.5A** top). For the theta/alpha PLV  
624 between the posterior hippocampus and the EC, we observed a higher PLV in load 6/8  
625 than load 4 (FDR corrected: load4 vs load6,  $p = 0.007$ ; load4 vs load8,  $p = 0.007$ ;



626 load6 vs load8,  $p = 0.86$ ; **Fig.5A** bottom). Regarding the theta/alpha GC index  
627 between the anterior hippocampus and the EC, we found a higher GC value from the  
628 anterior hippocampus to EC in the high load conditions compared to the low load  
629 condition (FDR corrected: load4 vs load6,  $p = 0.076$ ; load4 vs load8,  $p = 0.044$ ; load6  
630 vs load8,  $p = 0.43$ ; **Fig.5B** top). However, in the opposite direction, there were no  
631 significant differences observed (permutation test, all  $ps > 0.05$ ; **Fig.5B** bottom).  
632 Regarding to the theta/alpha GC index between the posterior hippocampus and the  
633 EC, we did not find any difference between loads in either direction (permutation test,  
634 all  $ps > 0.05$ ; **Fig.5C**). For the anterior hippocampal theta/alpha – EC gamma zPAC,  
635 no significant differences between loads were found (permutation test, all  $ps > 0.05$ ;  
636 **Fig.5D** top); for the posterior hippocampal theta/alpha – EC gamma zPAC, stronger  
637 coupling in high load condition was found relative to low load condition (FDR  
638 corrected, load4 vs load6,  $p = 0.026$ ; load4 vs load8,  $p = 0.047$ ; load6 vs load8,  $p =$   
639  $0.56$ ; **Fig.5D** bottom). In addition, we also directly compared measurements from the  
640 two directions under each load condition using paired  $t$ -tests, leading to no directional  
641 difference in any comparison (all  $ps > 0.05$ ). In summary, our observations indicate  
642 that WM load affects both the anterior and posterior hippocampus in a comparable  
643 manner, which is consistent with the impact of WM load on the connections between  
644 the entire hippocampus and the EC.

## 645 **Local Power Analysis for WM Load**

646 The above analyses revealed that the WM load can be decoded by the hippocampal-  
647 EC interactions in the theta/alpha band and in the theta/alpha-gamma coupling. We  
648 next asked whether local activity in the hippocampus and the EC indicate WM load.  
649 We calculated the time-frequency power for each channel separately for trials with  
650 load4, 6 and 8. The power outputs were  $z$ -scored against the pretrial baseline  
651 distributions to assess the significance of the task-induced power effects per trial (see  
652 **Methods**). We separately calculated the  $z$ -scored power within the hippocampus and  
653 EC in the theta/alpha band for each load in each participant and fed the power features  
654 into the SVM classifier to decode the WM load with LOOCV. As shown in **Fig.6A**,  
655 no significant results were found for any of the regions for the classification of WM  
656 load (Hipp:  $41.03\% \pm 5.54\%$ ; EC:  $46.15\% \pm 6.01\%$ ; permutation test against  
657 scrambled labels,  $p > 0.05$ ). This analysis indicated that the load effects on  
658 hippocampal-entorhinal interaction were not significantly explained by load effect on  
659 the power at hippocampal or entorhinal channels. We would like to stress that these  
660 results do not exclude a role of local activity.

661

662 As previous studies noted (Donoghue and Watrous, 2023), the conventional analytical  
663 approaches concerning neural oscillatory activity have a tendency to conflate periodic  
664 and aperiodic activities. To test whether the impact of aperiodic activity could explain  
665 our observations of functional effects, we first extracted the aperiodic activity using

666 FOOOF toolbox (Donoghue et al., 2020b) from the hippocampus and EC for each  
667 load and participant and then conducted a repeated-measures ANOVA with a within-  
668 group effect of load across the frequency spectrum. Results indicated that the  
669 aperiodic activity did not exhibit significant differences among WM loads (all  $p$ s >  
670 0.05, **Fig. 6B**). Next, we added the aperiodic activity as a regressor in the analysis of  
671 functional effects of hippocampal theta/alpha phase – EC gamma amplitude  $z$ PAC  
672 (see Methods for details). The load was still significant to  $z$ PAC (linear mixed-effects  
673 model,  $p = 0.011$ ,  $t = 2.71$ ), even when controlling for the aperiodic activity of the  
674 hippocampus in the theta/alpha range ( $p = 0.43$ ) and of the EC in the gamma range ( $p$   
675 = 0.07). This result validated our previous findings that the modulation of the  
676 hippocampal theta/alpha phase on the EC gamma amplitude carries the load  
677 information. To further rule out the bias of aperiodic activity on the information flow  
678 between the hippocampus and the EC, we did similar analysis for GC index (see  
679 Methods for details). Our finding noted that the effect of load was significantly  
680 associated with hippocampal driven GC (linear mixed-effects model,  $p = 0.024$ ,  $t =$   
681 2.82), while neither the aperiodic activity from the hippocampus ( $p = 0.35$ ) nor those  
682 from the EC ( $p = 0.54$ ) significantly contributed to it. Then, we did a similar analysis  
683 with EC driven GC as dependent variable, none of the effects, including load and  
684 aperiodic activity in either region, reached statistical significance (all  $p$ s > 0.05). This  
685 result replicates our previous findings and underscores the influence of WM load on  
686 hippocampal driven GC, even when controlling for aperiodic components.

687

688

689 In summary, WM maintenance was accompanied with elevated synchrony within the  
690 hippocampal-entorhinal interaction, with a theta/alpha coordinated hippocampal-  
691 driven influence on the EC. This influence, including information transfer from the  
692 hippocampus to the EC in theta/alpha band and the hippocampal theta/alpha phase  
693 entraining EC gamma amplitude, increased from WM low load (load4) to high load  
694 conditions (load6/8), and predicted WM load (**Fig.6C**).

695

## 696 **Discussion**

697 We showed that WM maintenance is associated with coordinated neural oscillations  
698 between the hippocampus and the EC in specific oscillatory modes of frequency and  
699 direction. In particular, we observed increased hippocampal driven information  
700 transfer via the theta/alpha band, and increased PAC between the theta/alpha phase of  
701 the hippocampus entraining the gamma amplitude of the EC. This inter-regional  
702 communication during maintenance increased with WM load and predicted WM load.  
703 These findings provided direct neural evidence of hippocampal-EC interactions  
704 during WM maintenance in humans and links a specific inter-regional activity pattern  
705 to WM load.

706

707 The interregional oscillatory dynamics are consistent with known structural and  
708 functional connections between the hippocampus and the EC. Anatomical studies  
709 found that the EC sends projections to and receives monosynaptic input from the  
710 hippocampus (van Groen et al., 2003; Small et al., 2011). Optogenetic inhibition of  
711 this circuit in mice resulted reduction in both inter-regional connectivity and the  
712 correct execution of WM-guided behavior (Yamamoto et al., 2014). Our results are  
713 thus consistent with animal literature suggesting the contribution of hippocampal-EC  
714 communication to WM processing and extended these findings to humans.

715

716 To investigate this communication, we computed the hippocampal-EC phase  
717 synchronization, a neural mechanism that is thought to enhance neural  
718 communication and plasticity (Fell and Axmacher, 2011; Daume et al., 2023).  
719 Consistent with this notion, previous studies have shown that theta/alpha band phase  
720 synchronization facilitates the recruitment of WM-related regions, including various  
721 cortical areas (Johnson et al., 2018b) as well as the hippocampus and cortical areas  
722 (Boran et al., 2019; Dimakopoulos et al., 2022), thereby supporting WM function.

723

724 To date, only a handful of human studies have collected direct intracranial data on  
725 both the hippocampus and the EC during WM processing, and all looked at each  
726 region separately rather than at their connectivity (Kornblith et al., 2017; Boran et al.,  
727 2019; Boran et al., 2022). Considering the evidence for decoding WM load through

728 inter-regional interaction in the present study, our findings point to a coordinated role  
729 of the hippocampus and the EC in WM information maintenance. These results  
730 underscore the significance of investigating connections to understand the neural  
731 mechanisms of WM. Our results align with animal findings mapping the non-spatial  
732 dimension of the hippocampal-EC circuit (Aronov et al., 2017). They together suggest  
733 a common circuit mechanism that contribute to diverse behavioral tasks and  
734 supporting cognitive processes beyond spatial navigation.

735

736 Both the GC and PSI measures, despite being based on different principles  
737 (magnitude and phase), consistently demonstrated that the net information flow is  
738 from the hippocampus to the EC during WM maintenance. This is in agreement with  
739 animal results where the hippocampus receives sensory information from the EC  
740 during encoding and subsequently processes and returns memory-related information  
741 (Buzsáki and Tingley, 2018; Rozov et al., 2020). The hippocampal outflow during  
742 WM maintenance may also contribute to the transfer of memories from short-term  
743 storage in the hippocampus to long-term storage in the neocortex as part of the  
744 memory consolidation process (Frankland and Bontempi, 2005; Kaminski and  
745 Rutishauser, 2020). These findings provide further confirmation of the directional  
746 modulation observed in humans and point to a role of neural oscillations in regulating  
747 this modulation. Recent studies found that memory consolidation may start as early as  
748 at the end of encoding (Ben-Yakov et al., 2013; Zhang et al., 2021). In agreement

749 with this, hippocampal outflow during the post-encoding period can decode  
750 subsequent memory performance (Zhang et al., 2021), and WM maintenance  
751 contributes to long-term memory performance (Ranganath et al., 2005; Kaminski and  
752 Rutishauser, 2020). Taken together, our results may have implications in  
753 understanding long-term memory consolidation.

754

755 The theta/alpha oscillations drive inter-regional communication in the hippocampal-  
756 EC circuit during WM maintenance. Previous studies reported theta/alpha frequency  
757 synchronization between the hippocampus and cortical regions (Johnson et al., 2018b;  
758 Dimakopoulos et al., 2022) and between cortical regions (Johnson et al., 2018a)  
759 during WM maintenance. Computational models have suggested that these  
760 oscillations coordinate the proper timing of interactions between the hippocampus and  
761 the EC (Kurikawa et al., 2021). Here, we speculate that, during WM maintenance,  
762 task-relevant mnemonic signals are strengthened by theta connectivity, and stronger  
763 distracting signals are suppressed by higher levels of alpha synchronization. Rodent  
764 studies showed that these oscillations in the hippocampal-EC circuit facilitate synaptic  
765 plasticity (Diana et al., 2007; Buzsaki and Moser, 2013; Colgin, 2013). Human iEEG  
766 studies reported that the hippocampal-EC communications via the theta band  
767 contributed to episodic memory (Solomon et al., 2019). We extend these findings to  
768 WM by reporting a load-dependent increase in the hippocampal-EC connectivity.

769

770 In subsequent analysis involving cross-frequency coupling features, we observed that  
771 WM load was associated with theta/alpha-gamma phase-amplitude couplings (PACs)  
772 in the hippocampal-EC circuit. Previous studies have consistently highlighted the  
773 involvement of rhythmic activity at theta, alpha, and gamma frequencies in WM  
774 maintenance (Bragin et al., 1995; Sarnthein et al., 1997; Axmacher et al., 2007;  
775 Michels et al., 2008; Roux and Uhlhaas, 2014; Daume et al., 2023). Theta-gamma  
776 PAC has been proposed to modulate synaptic plasticity (Huerta and Lisman, 1995)  
777 and organize complex mnemonic information (Heusser et al., 2016), while alpha-  
778 gamma PAC has been implicated in the gating of sensory information and read-out of  
779 relevant WM items (Roux et al., 2013; Davoudi et al., 2021). Cross-regional PAC  
780 describes coordinated brain activity between brain regions. However, it is important  
781 to note that the presence of cross-regional PAC does not imply directional causality.  
782 Canolty and Knight (2010) introduced a model explaining how synchronized theta  
783 oscillations and local PAC regulate cortical activity in relation to the hippocampus,  
784 suggesting that inter-regional cross-regional PAC is a secondary outcome of this  
785 cortical organization. Drawing upon the functional roles of local theta/alpha-gamma  
786 PACs mentioned above, we hypothesize that cross-regional PAC may serve as a  
787 mechanism for the formation of an integrated memory representation through precise  
788 coordination of local high-frequency oscillations. Besides, coupling between  
789 hippocampal theta phase and gamma activity in the EC, in the same frequency band  
790 and direction as found in our study, was suggested supporting episodic memory  
791 (Wang et al., 2021). Our study extends this finding to WM and they together imply



792 the cross-regional PAC as a key neurophysiological mechanism in mnemonic  
793 processing.

794

795 Besides, we found distinctions in inter-regional interaction patterns between low and  
796 high WM load conditions. This pattern aligns with our earlier research (Boran et al.,  
797 2019), which demonstrated that load-sensitive maintenance neurons in the  
798 hippocampus exhibited a plateauing effect at high-load levels rather than showing  
799 incremental increases of firing rates with WM load. However, we do not interpret this  
800 as reflecting a binary relationship between inter-regional connectivity and WM load.  
801 Instead, this observation may suggest the presence of processing capacity limits (von  
802 Allmen et al., 2013), which are closely tied to the concept of workload. We reported  
803 that the averaged capacity was 7.2 (see Results), indicating that participants were  
804 capable of maintaining at least seven letters in memory. However, when attempting to  
805 maintain 8 letters, they may reach or exceed their capacity limits. Consequently, we  
806 might not observe further elevation in inter-regional connectivity.

807

808 In summary, our results provide direct evidence that WM maintenance is supported  
809 by the unidirectional influence from the hippocampus to the EC via the theta/alpha  
810 band in a load-dependent manner. We have extended previous knowledge of the  
811 contribution of the hippocampal-EC circuit on WM in animals to humans.

812

813 **Data availability**

814 The data set was analyzed and described earlier (Boran et al., 2019; Boran et al.,  
815 2020; Dimakopoulos et al., 2022; Li et al., 2022; Li et al., 2023a) and is freely  
816 available for download at <https://doi.gin.g-node.org/10.12751/g-node.d76994/>. The  
817 task is freely available for download at  
818 [http://www.neurobs.com/ex\\_files/expt\\_view?id=266](http://www.neurobs.com/ex_files/expt_view?id=266). Links to updates and further  
819 data sets can be found at <https://hfozuri.ch>.

820

JNeurosci Accepted Manuscript

# References

- Aronov D, Nevers R, Tank DW (2017) Mapping of a non-spatial dimension by the hippocampal-entorhinal circuit. *Nature* 543:719-722.
- Axmacher N, Mormann F, Fernandez G, Cohen MX, Elger CE, Fell J (2007) Sustained neural activity patterns during working memory in the human medial temporal lobe. *J Neurosci* 27:7807-7816.
- Axmacher N, Henseler MM, Jensen O, Weinreich I, Elger CE, Fell J (2010) Cross-frequency coupling supports multi-item working memory in the human hippocampus. *Proc Natl Acad Sci U S A* 107:3228-3233.
- Baddeley A (2007) *Working memory, thought, and action*: OuP Oxford.
- Baddeley A (2012) Working memory: theories, models, and controversies. *Annu Rev Psychol* 63:1-29.
- Barnett L, Seth AK (2014) The MVGC multivariate Granger causality toolbox: a new approach to Granger-causal inference. *Journal of neuroscience methods* 223:50-68.
- Ben-Yakov A, Eshel N, Dudai Y (2013) Hippocampal immediate poststimulus activity in the encoding of consecutive naturalistic episodes. *J Exp Psychol Gen* 142:1255-1263.
- Boran E, Hilfiker P, Stieglitz L, Sarnthein J, Klaver P (2022) Persistent neuronal firing in the medial temporal lobe supports performance and workload of visual working memory in humans. *Neuroimage* 254:119123.
- Boran E, Fedele T, Klaver P, Hilfiker P, Stieglitz L, Grunwald T, Sarnthein J (2019) Persistent hippocampal neural firing and hippocampal-cortical coupling predict verbal working memory load. *Sci Adv* 5:eaav3687.
- Boran E, Fedele T, Steiner A, Hilfiker P, Stieglitz L, Grunwald T, Sarnthein J (2020) Dataset of human medial temporal lobe neurons, scalp and intracranial EEG during a verbal working memory task. *Sci Data* 7:30.
- Bragin A, Jando G, Nadasdy Z, Hetke J, Wise K, Buzsáki G (1995) Gamma (40-100 Hz) oscillation in the hippocampus of the behaving rat. *J Neurosci* 15:47-60.
- Buzsáki G, Moser EI (2013) Memory, navigation and theta rhythm in the hippocampal-entorhinal system. *Nat Neurosci* 16:130-138.
- Buzsáki G (2002) Theta oscillations in the hippocampus. *Neuron* 33:325-340.
- Buzsáki G, Tingley D (2018) Space and Time: The Hippocampus as a Sequence Generator. *Trends Cogn Sci* 22:853-869.

- Canolty RT, Knight RT (2010) The functional role of cross-frequency coupling. *Trends Cogn Sci* 14:506-515.
- Chang C-C, Lin C-J (2011) LIBSVM: a library for support vector machines. *ACM transactions on intelligent systems and technology (TIST)* 2:1-27.
- Christophel TB, Klink PC, Spitzer B, Roelfsema PR, Haynes JD (2017) The Distributed Nature of Working Memory. *Trends Cogn Sci* 21:111-124.
- Cohen MX (2014) *Analyzing neural time series data: theory and practice*: MIT press.
- Colgin LL (2013) Mechanisms and functions of theta rhythms. *Annu Rev Neurosci* 36:295-312.
- Colgin LL (2016) Rhythms of the hippocampal network. *Nat Rev Neurosci* 17:239-249.
- Cowan N (2001) The magical number 4 in short-term memory: a reconsideration of mental storage capacity. *Behav Brain Sci* 24:87-114; discussion 114-185.
- Daume J, Kaminski J, Schjetnan AGP, Salimpour Y, Khan U, Reed C, Anderson W, Valiante TA, Mamelak AN, Rutishauser U (2023) Control of working memory maintenance by theta-gamma phase amplitude coupling of human hippocampal neurons. *bioRxiv*.
- Davoudi S, Parto Dezfouli M, Knight RT, Daliri MR, Johnson EL (2021) Prefrontal Lesions Disrupt Posterior Alpha-Gamma Coordination of Visual Working Memory Representations. *J Cogn Neurosci* 33:1798-1810.
- Diana RA, Yonelinas AP, Ranganath C (2007) Imaging recollection and familiarity in the medial temporal lobe: a three-component model. *Trends Cogn Sci* 11:379-386.
- Dimakopoulos V, Mégevand P, Stieglitz LH, Imbach L, Sarnthein J (2022) Information flows from hippocampus to auditory cortex during replay of verbal working memory items. *Elife* 11.
- Donoghue T, Watrous AJ (2023) How can we differentiate narrow-band oscillations from aperiodic activity? In: *Intracranial EEG: A Guide for Cognitive Neuroscientists*, pp 351-364: Springer.
- Donoghue T, Dominguez J, Voytek B (2020a) Electrophysiological frequency band ratio measures conflate periodic and aperiodic neural activity. *Eneuro* 7.
- Donoghue T, Haller M, Peterson EJ, Varma P, Sebastian P, Gao R, Noto T, Lara AH, Wallis JD, Knight RT (2020b) Parameterizing neural power spectra into periodic and aperiodic components. *Nature neuroscience* 23:1655-1665.
- Fan L, Li H, Zhuo J, Zhang Y, Wang J, Chen L, Yang Z, Chu C, Xie S, Laird AR, Fox PT, Eickhoff SB, Yu C, Jiang T (2016) The Human Brainnetome Atlas: A New Brain Atlas Based on Connectional Architecture. *Cereb Cortex* 26:3508-3526.
- Fell J, Axmacher N (2011) The role of phase synchronization in memory processes. *Nat Rev Neurosci* 12:105-118.

- Fell J, Ludowig E, Staresina BP, Wagner T, Kranz T, Elger CE, Axmacher N (2011) Medial temporal theta/alpha power enhancement precedes successful memory encoding: evidence based on intracranial EEG. *J Neurosci* 31:5392-5397.
- Frankland PW, Bontempi B (2005) The organization of recent and remote memories. *Nat Rev Neurosci* 6:119-130.
- Hasselmo ME, Bodelon C, Wyble BP (2002) A proposed function for hippocampal theta rhythm: separate phases of encoding and retrieval enhance reversal of prior learning. *Neural Comput* 14:793-817.
- Heusser AC, Poeppel D, Ezzyat Y, Davachi L (2016) Episodic sequence memory is supported by a theta-gamma phase code. *Nat Neurosci* 19:1374-1380.
- Huerta PT, Lisman JE (1995) Bidirectional synaptic plasticity induced by a single burst during cholinergic theta oscillation in CA1 in vitro. *Neuron* 15:1053-1063.
- Johnson EL, King-Stephens D, Weber PB, Laxer KD, Lin JJ, Knight RT (2018a) Spectral Imprints of Working Memory for Everyday Associations in the Frontoparietal Network. *Front Syst Neurosci* 12:65.
- Johnson EL, Adams JN, Solbakk AK, Endestad T, Larsson PG, Ivanovic J, Meling TR, Lin JJ, Knight RT (2018b) Dynamic frontotemporal systems process space and time in working memory. *PLoS Biol* 16:e2004274.
- Kaminski J, Rutishauser U (2020) Between persistently active and activity-silent frameworks: novel vistas on the cellular basis of working memory. *Ann N Y Acad Sci* 1464:64-75.
- Kaminski J, Sullivan S, Chung JM, Ross IB, Mamelak AN, Rutishauser U (2017) Persistently active neurons in human medial frontal and medial temporal lobe support working memory. *Nat Neurosci* 20:590-601.
- Kornblith S, Quiñan Quiroga R, Koch C, Fried I, Mormann F (2017) Persistent Single-Neuron Activity during Working Memory in the Human Medial Temporal Lobe. *Curr Biol* 27:1026-1032.
- Kumar B, Gupta D (2021) Universum based Lagrangian twin bounded support vector machine to classify EEG signals. *Comput Methods Programs Biomed* 208:106244.
- Kurikawa T, Mizuseki K, Fukai T (2021) Oscillation-Driven Memory Encoding, Maintenance, and Recall in an Entorhinal-Hippocampal Circuit Model. *Cereb Cortex* 31:2038-2057.
- Lavenex P, Amaral DG (2000) Hippocampal-neocortical interaction: a hierarchy of associativity. *Hippocampus* 10:420-430.
- Li J, Cao D, Yu S, Xiao X, Imbach L, Stieglitz L, Sarnthein J, Jiang T (2023a) Functional specialization and interaction in the amygdala-hippocampus circuit during working memory processing. *Nat Commun* 14:2921.

- Li J, Cao D, Yu S, Xiao X, Imbach L, Stieglitz L, Sarnthein J, Jiang T (2023b) Functional specialization and interaction in the amygdala-hippocampus circuit during working memory processing. *Nature Communications* 14:2921.
- Li J, Cao D, Dimakopoulos V, Shi W, Yu S, Fan L, Stieglitz L, Imbach L, Sarnthein J, Jiang T (2022) Anterior-Posterior Hippocampal Dynamics Support Working Memory Processing. *J Neurosci* 42:443-453.
- Mamashli F, Khan S, Hamalainen M, Jas M, Raji T, Stufflebeam SM, Nummenmaa A, Ahveninen J (2021) Synchronization patterns reveal neuronal coding of working memory content. *Cell Rep* 36:109566.
- Michels L, Moazami-Goudarzi M, Jeanmonod D, Sarnthein J (2008) EEG alpha distinguishes between cuneal and precuneal activation in working memory. *NeuroImage* 40:1296-1310.
- Nolte G, Ziehe A, Nikulin VV, Schlögl A, Krämer N, Brismar T, Müller KR (2008) Robustly estimating the flow direction of information in complex physical systems. *Phys Rev Lett* 100:234101.
- Oehrns CR, Hanslmayr S, Fell J, Deuker L, Kremers NA, Do Lam AT, Elger CE, Axmacher N (2014) Neural communication patterns underlying conflict detection, resolution, and adaptation. *J Neurosci* 34:10438-10452.
- Oostenveld R, Fries P, Maris E, Schoffelen JM (2011) FieldTrip: Open source software for advanced analysis of MEG, EEG, and invasive electrophysiological data. *Comput Intell Neurosci* 2011:156869.
- Oosterhof NN, Connolly AC, Haxby JV (2016) CoSMoMVPA: Multi-Modal Multivariate Pattern Analysis of Neuroimaging Data in Matlab/GNU Octave. *Front Neuroinform* 10:27.
- Pacheco Estefan D, Sánchez-Fibla M, Duff A, Principe A, Rocamora R, Zhang H, Axmacher N, Verschure P (2019) Coordinated representational reinstatement in the human hippocampus and lateral temporal cortex during episodic memory retrieval. *Nat Commun* 10:2255.
- Poldrack RA (2011) Inferring mental states from neuroimaging data: from reverse inference to large-scale decoding. *Neuron* 72:692-697.
- Poldrack RA, Halchenko YO, Hanson SJ (2009) Decoding the large-scale structure of brain function by classifying mental states across individuals. *Psychological science* 20:1364-1372.
- Ranganath C, Cohen MX, Brozinsky CJ (2005) Working memory maintenance contributes to long-term memory formation: neural and behavioral evidence. *J Cogn Neurosci* 17:994-1010.
- Rosene DL, Van Hoesen GW (1977) Hippocampal efferents reach widespread areas of cerebral cortex and amygdala in the rhesus monkey. *Science* 198:315-317.
- Roux F, Uhlhaas PJ (2014) Working memory and neural oscillations: alpha-gamma versus theta-gamma codes for distinct WM information? *Trends Cogn Sci* 18:16-25.

- Roux F, Wibral M, Singer W, Aru J, Uhlhaas PJ (2013) The phase of thalamic alpha activity modulates cortical gamma-band activity: evidence from resting-state MEG recordings. *J Neurosci* 33:17827-17835.
- Rozov A, Rannap M, Lorenz F, Nasretdinov A, Draguhn A, Egorov AV (2020) Processing of Hippocampal Network Activity in the Receiver Network of the Medial Entorhinal Cortex Layer V. *J Neurosci* 40:8413-8425.
- Sarnthein J, vonStein A, Rappelsberger P, Petsche H, Rauscher FH, Shaw GL (1997) Persistent patterns of brain activity: an EEG coherence study of the positive effect of music on spatial-temporal reasoning. *Neurol Res* 19:107-116.
- Small SA, Schobel SA, Buxton RB, Witter MP, Barnes CA (2011) A pathophysiological framework of hippocampal dysfunction in ageing and disease. *Nat Rev Neurosci* 12:585-601.
- Solomon EA, Stein JM, Das S, Gorniak R, Sperling MR, Worrell G, Inman CS, Tan RJ, Jobst BC, Rizzuto DS, Kahana MJ (2019) Dynamic Theta Networks in the Human Medial Temporal Lobe Support Episodic Memory. *Curr Biol* 29:1100-1111 e1104.
- Squire LR (1992) Memory and the hippocampus: a synthesis from findings with rats, monkeys, and humans. *Psychol Rev* 99:195-231.
- Suh J, Rivest AJ, Nakashiba T, Tominaga T, Tonegawa S (2011) Entorhinal cortex layer III input to the hippocampus is crucial for temporal association memory. *Science* 334:1415-1420.
- Suzuki WA, Miller EK, Desimone R (1997) Object and place memory in the macaque entorhinal cortex. *J Neurophysiol* 78:1062-1081.
- Tort AB, Komorowski R, Eichenbaum H, Kopell N (2010) Measuring phase-amplitude coupling between neuronal oscillations of different frequencies. *J Neurophysiol* 104:1195-1210.
- van Groen T, Miettinen P, Kadish I (2003) The entorhinal cortex of the mouse: organization of the projection to the hippocampal formation. *Hippocampus* 13:133-149.
- Vaz AP, Yaffe RB, Wittig JH, Jr., Inati SK, Zaghoul KA (2017) Dual origins of measured phase-amplitude coupling reveal distinct neural mechanisms underlying episodic memory in the human cortex. *Neuroimage* 148:148-159.
- von Allmen DY, Wurmitzer K, Martin E, Klaver P (2013) Neural activity in the hippocampus predicts individual visual short-term memory capacity. *Hippocampus* 23:606-615.
- Wang DX, Schmitt K, Seger S, Davila CE, Lega BC (2021) Cross-regional phase amplitude coupling supports the encoding of episodic memories. *Hippocampus* 31:481-492.
- Wong T-T (2015) Performance evaluation of classification algorithms by k-fold and leave-one-out cross validation. *Pattern Recognition* 48:2839-2846.

- Xia M, Wang J, He Y (2013) BrainNet Viewer: a network visualization tool for human brain connectomics. *PLoS One* 8:e68910.
- Yamamoto J, Suh J, Takeuchi D, Tonegawa S (2014) Successful execution of working memory linked to synchronized high-frequency gamma oscillations. *Cell* 157:845-857.
- Yamashita M, Yoshihara Y, Hashimoto R, Yahata N, Ichikawa N, Sakai Y, Yamada T, Matsukawa N, Okada G, Tanaka SC, Kasai K, Kato N, Okamoto Y, Seymour B, Takahashi H, Kawato M, Imamizu H (2018) A prediction model of working memory across health and psychiatric disease using whole-brain functional connectivity. *Elife* 7.
- Young BJ, Otto T, Fox GD, Eichenbaum H (1997) Memory representation within the parahippocampal region. *J Neurosci* 17:5183-5195.
- Zhang H, Skelin I, Ma S, Paff M, Yassa MA, Knight RT, Lin JJ (2021) Awake ripples enhance emotional memory encoding in the human brain. *bioRxiv:2021.2011.2017.469047*.
- Zhang SJ, Ye J, Miao C, Tsao A, Cerniauskas I, Ledergerber D, Moser MB, Moser EI (2013) Optogenetic dissection of entorhinal-hippocampal functional connectivity. *Science* 340:1232627.
- Zheng J, Stevenson RF, Mander BA, Mnatsakanyan L, Hsu FPK, Vadera S, Knight RT, Yassa MA, Lin JJ (2019) Multiplexing of Theta and Alpha Rhythms in the Amygdala-Hippocampal Circuit Supports Pattern Separation of Emotional Information. *Neuron* 102:887-898 e885.



**Table 1 Subject characteristics**

Participant	Age	Sex	EC sites	Hippocampal sites	Response accuracy % for load4	Response accuracy % for load6	Response accuracy % for load8	Number of trials (sessions)
-------------	-----	-----	----------	-------------------	-------------------------------	-------------------------------	-------------------------------	-----------------------------

1	24	Female	2	6	100	92	85	200 (4)
2	39	Male	4	8	96	81	79	339 (7)
3	18	Female	2	6	98	94	89	147 (3)
4	28	Male	4	8	100	94	89	99 (2)
5	31	Male	4	8	99	91	91	349 (6)
6	47	Male	4	8	99	92	93	197 (4)
7	56	Female	4	7	97	96	75	249 (5)
8	19	Female	4	8	100	94	85	96 (2)
9	35	Male	4	6	99	92	87	199 (4)
10	51	Female	4	6	96	91	86	382 (8)
11	30	Male	4	4	98	88	78	200 (4)
12	29	Female	2	4	98	100	95	295 (6)

JNeurosci Accepted Manuscript

# Figure legends

## **Fig. 1 Working memory task, recording sites, and schematic of multivariate pattern analysis.**

(A) An example trial of the task. Each trial consisted of a set of consonants, including four, six or eight letters for 2 s (encoding). The number of letters was thus specific for the memory load (load 4, load 6 and load 8). After a delay for 3 s (maintenance, red), a probe letter was shown, and the participants indicated whether the probe was or was not contained in the stimulus letter set.

(B) Response accuracy decreased with load 4 (light red), 6 (light green) and 8 (light blue) across the group of participants. \*\*  $p < 0.01$ .

(C) Channel locations of all participants in MNI152 space. Recording regions are indicated by different colors (red, hippocampus; blue, EC).

(D) Schematic of the multivariate pattern analysis. Phase locking value (PLV), Granger causality index (GC), and phase-amplitude coupling (PAC) were calculated separately between the Hipp (red) and the EC (blue) for trials with WM load 4, load 6 and load 8. The patterns of PLV (e.g., theta/alpha PLV), GC (e.g., theta/alpha GC) and PAC (e.g., theta/alpha-gamma PAC) were separately used to train the support vector machine (SVM) classifier to classify the WM load (load 4, load 6 or load 8).

Specifically, we converted the features to a feature vector ( $M$ ), fed them into a linear SVM classifier, trained the classifier on the data from  $N-1$  participants ( $(N-1) \times M$ ), and tested it on the remaining one participant ( $1 \times M$ ). We used inter-participant cross validation by leaving one participant out for validation and replicated the classification. The accuracy was used as the performance metric.

**Fig. 2 Frequency-specific hippocampus-EC phase locking value (PLV) during maintenance is load sensitive.**

(A) Phase synchrony (PLV) between the hippocampus and the EC was identified across all participants for the load 4 (left), load 6 (middle) and load 8 (right) conditions, with greater low-frequency synchrony during maintenance of WM load. The PLV ranged from 0 to 1, with warmer colors indicating higher PLV. The PLV maps show the PLV up to 12 Hz that survived the threshold from trials with load8 at  $p < 0.05$  (permutation test).

(B) Spectral PLV across the time domain within 1-100 Hz between the hippocampus and the EC across participants for the load 4 (light red), load 6 (light green) and load 8 (light blue) conditions (SEM shown as shaded area around the mean trace) with peaks in the theta/alpha range (2-12 Hz, light gray area) used for subsequent analyses. Black line indicates the threshold from the permutation test on the PLV with trials of load8.

(C) Significant increase in the PLV with trials of load6 (left panel) and load8 (right panel) related to the PLV with trials of load4 in the theta/alpha (2-12 Hz) frequency range during maintenance (cluster-based permutation,  $p < 0.05$ ). Warmer color denotes the work-load increase in the time-frequency space of PLV.

(D) Theta/alpha PLV of the hippocampus-EC across all participants in load 4, load 6 and load 8. The synchronization was larger in higher loads than in load 4.  $** p < 0.01$ .

(E) Decoding accuracy based on the theta/alpha PLV features between the hippocampus and the EC. The left panel shows the null distribution of the statistic for the decoding analysis, which were created using classifiers with randomized training labels. The threshold of significance is marked with a vertical dashed line ( $p < 0.05$ ). The right panel shows the decoding accuracy for WM load by using the theta/alpha PLV, the accuracy was above the threshold (horizontal dashed line, labeled with asterisk, \*  $p < 0.05$ ).

JNeurosci Accepted Manuscript

**Fig. 3 Information flow between the hippocampus and the EC reflects WM load.**

(A) Averaged GC index in the theta/alpha band from the Hippocampus to the EC (left) as well as from the opposite direction (right) across all participants for load4 (light red), load6 (light green), and load8 (light blue). Higher WM load was associated with increased GC from the hippocampus to EC, but not in the opposite direction. \*  $p < 0.05$ , #  $0.05 < p < 0.1$ .

(B) Decoding accuracy using the GC features from the hippocampus to the EC (red) and from the opposite direction (blue), respectively. The left panel shows the null distribution of the maximum statistics for these decoding analyses, which were created using classifiers with randomized training labels. The threshold of significance is marked with a vertical dashed line ( $p < 0.05$ ). The right panel shows the decoding accuracy using the theta/alpha GC index from both directions. WM load could be decoded by using the GC features from the hippocampus to the EC but not in the opposite direction. \*  $p < 0.05$ .

(C) The  $z$ -scored phase slope index (PSI) in the theta/alpha band across all participants for the load 4, load 6 and load 8 conditions. Positive values indicate that the hippocampus leads the EC. The  $z$ -scored PSI in the high load conditions (load 6/8) is higher than the load 4 condition. \*\*  $p < 0.01$ , \*  $p < 0.05$ .

**Fig. 4 Cross-regional coupling between the hippocampus and the EC.**

(A) Average  $z$ -scored PAC between hippocampal phase and EC amplitude, with logarithmic frequency scaling on both phase and amplitude axes across participants for trials with load4, load6, and load8. Notably, there is conspicuous cross-regional  $z$ -scored PAC between hippocampal theta/alpha (2-12 Hz) phase and EC gamma (30-100 Hz) amplitude ( $|z| > 1.96$ , highlighted in red).

(B)  $z$ -scored PAC depicting EC phase - hippocampus amplitude coupling for trials with load4, load6, and load8. In the theta/alpha (2-12 Hz) phase and gamma (30-100 Hz) frequency range, no significant coupling is evident ( $|z| < 1.96$ , represented in white).

(C) Averaged theta/alpha-gamma  $z$ PAC across participants from both directions in load4 (light red), load6 (light green) and load8 (light blue) conditions. The coupling between the hippocampus theta/alpha phase and the EC gamma amplitude was larger in the high load conditions (load6/8) than the low load condition (load4). \*  $p < 0.05$ .

(D) Decoding accuracy for WM load by using the  $z$ PAC features from hippocampal theta/alpha phase and EC gamma amplitude. The decoding accuracy (red, right panel) reached a significant level (horizontal dashed line in the right panel), which is 95<sup>th</sup> percentile of the null distribution of decoding accuracy (left panel).



**Fig.5 Inter-regional connectivity between the anterior/posterior hippocampal subregion and EC.**

(A) Averaged theta/alpha PLV between the anterior (top panel)/posterior hippocampus (bottom panel) and the EC for trials with load4 (light red), load6 (light green) and load8 (light blue). \*\*  $p < 0.01$ , \*  $p < 0.05$ .

(B) GC value between the anterior hippocampus and the EC. Top panel: the GC value from the anterior hippocampus to the EC was higher in the high load condition (load6/8, light green/blue) than the low load condition (load4, light red). Bottom panel: the GC value from the EC to the anterior hippocampus did not show any significant differences between WM loads. \*  $p < 0.05$ , #  $0.05 < p < 0.1$ .

(C) GC values between the posterior hippocampus and the EC. Both the GC value from the posterior hippocampus to the EC (top panel) and the GC value from the EC (bottom panel) to the posterior hippocampus did not display significant differences across working memory loads.

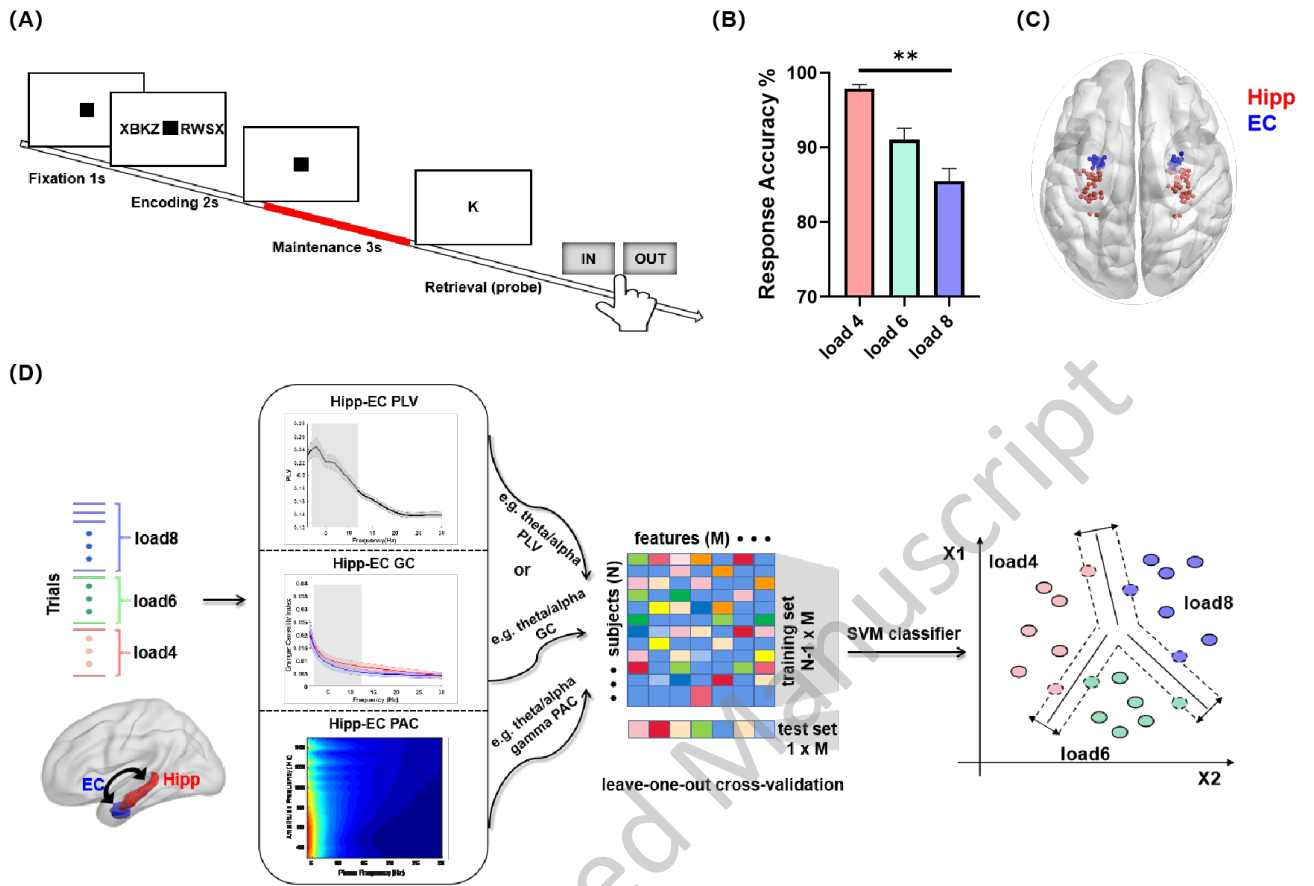
(D) The zPAC values with the theta/alpha phase of the anterior hippocampus modulating the gamma amplitude of the EC (top panel) did not show any differences between loads. While the zPAC values with the theta/alpha phase of the posterior hippocampus modulating the gamma amplitude of the EC (bottom panel) was higher in high load conditions (load6/8, light green/blue) compared to the load 4 condition (load4, light red). \*  $p < 0.05$ .

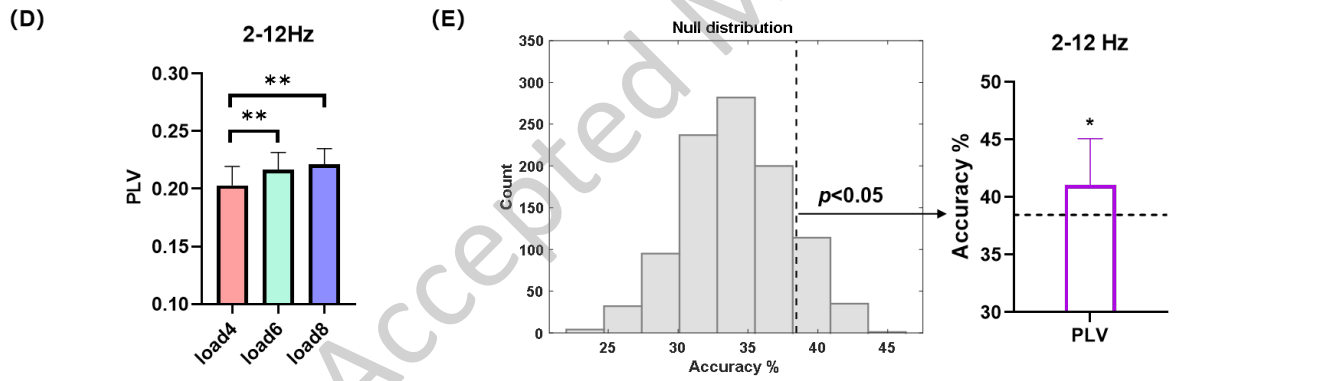
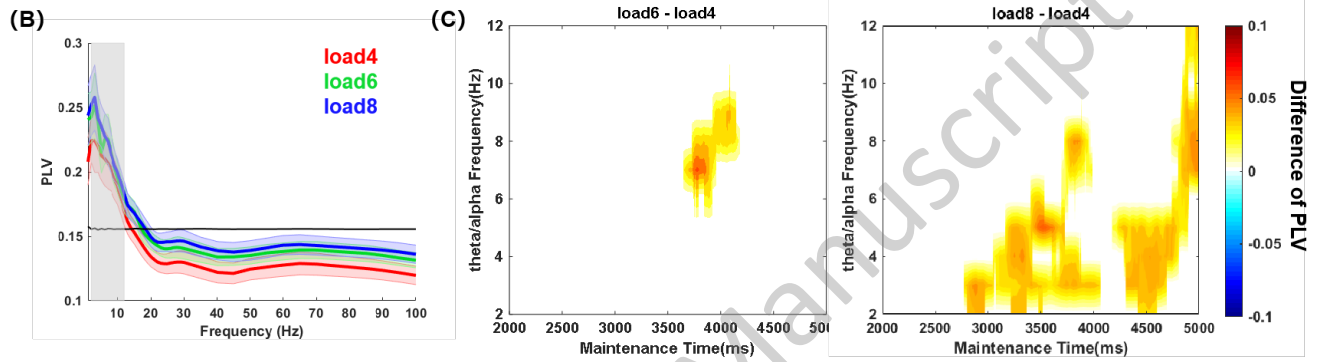
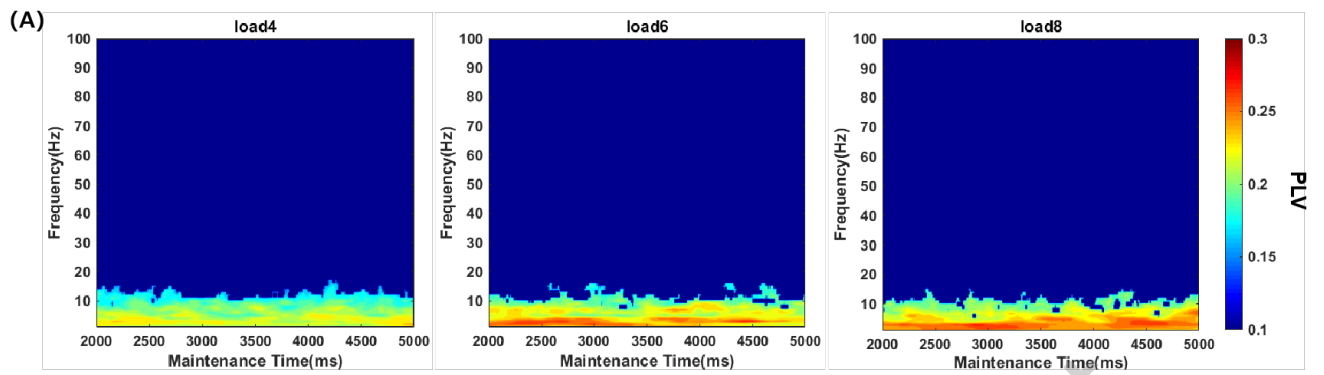
**Fig. 6 Hippocampal-entorhinal communications reflects WM load.**

(A) Decoding accuracy for WM load by using the theta/alpha power features within the hippocampus (red) and the EC (blue), respectively. The decoding accuracy in neither region exceeds the threshold of significance (dashed line,  $p < 0.05$ ).

(B) Aperiodic activity across the frequency spectrum from the hippocampus (left) and the EC (right). No difference was found among load4 (blue), load6 (green) and load8 (red). SEM shown as shaded area around the mean trace.

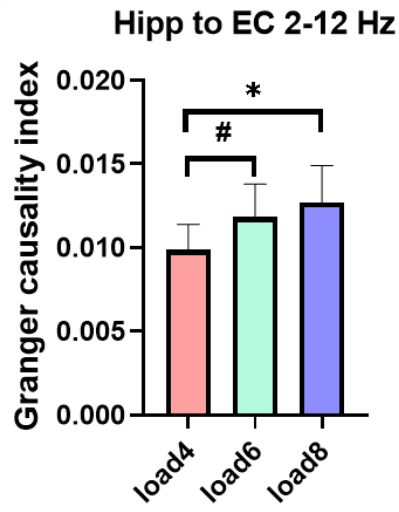
(C) Schematic of the hippocampal-entorhinal communications for low (top) and high (bottom) WM load. Unidirectional hippocampal influence on the EC increased with WM load via the theta/alpha band.



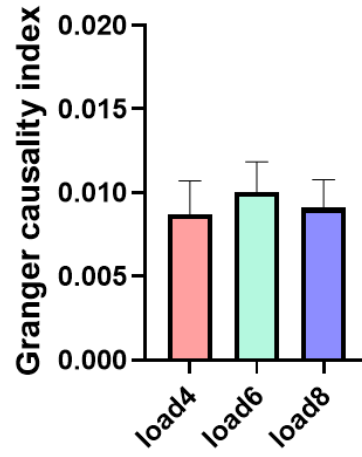


JNeurosci Accepted Manuscript

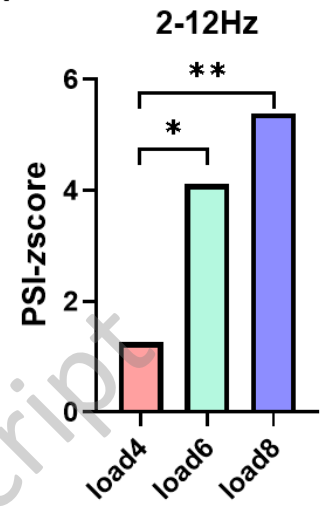
(A)



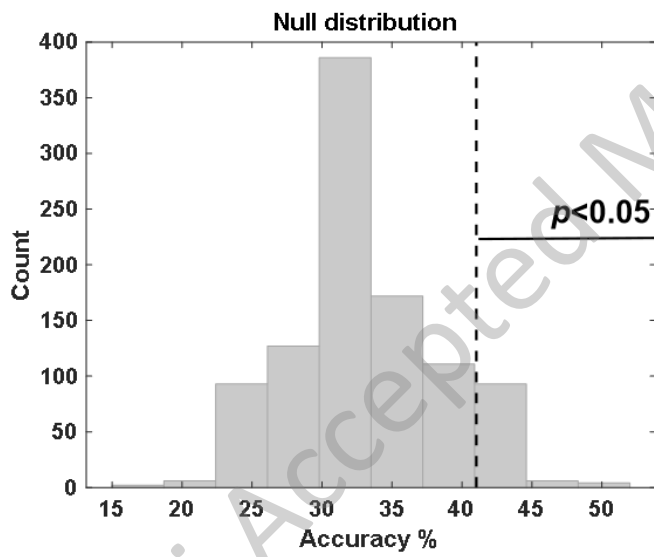
EC to Hipp 2-12 Hz



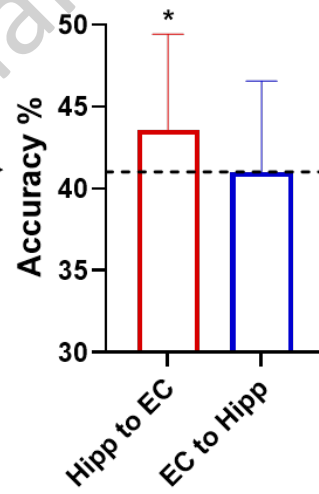
(C)

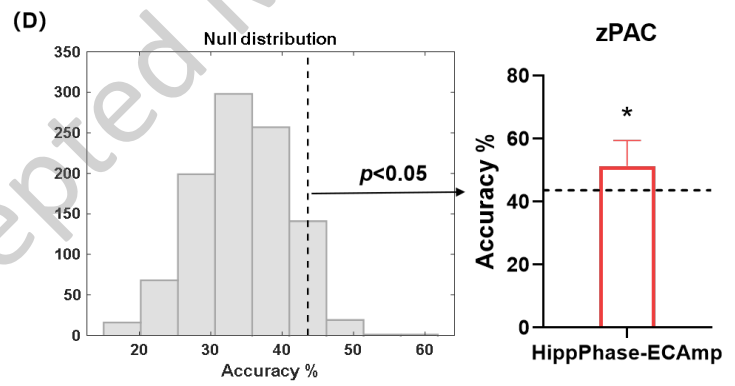
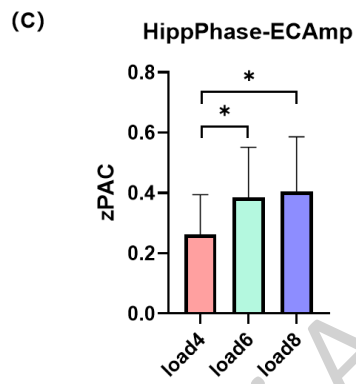
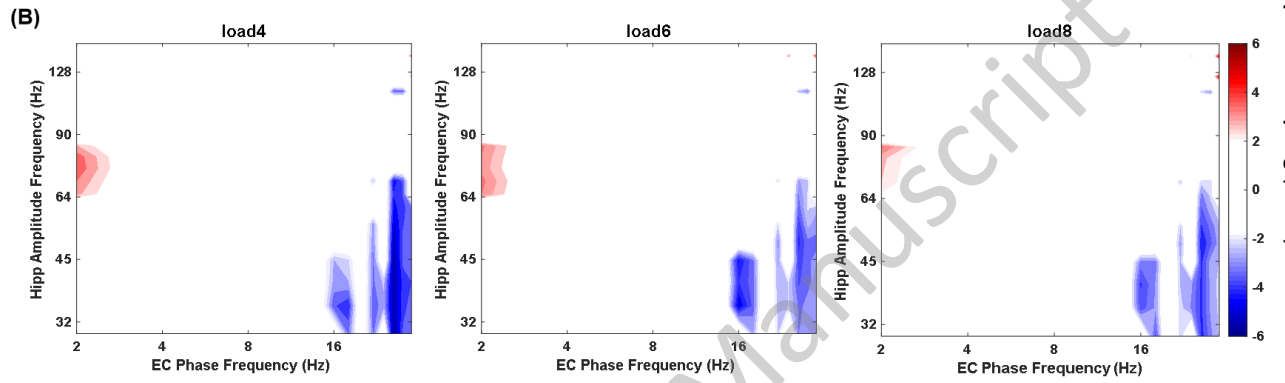
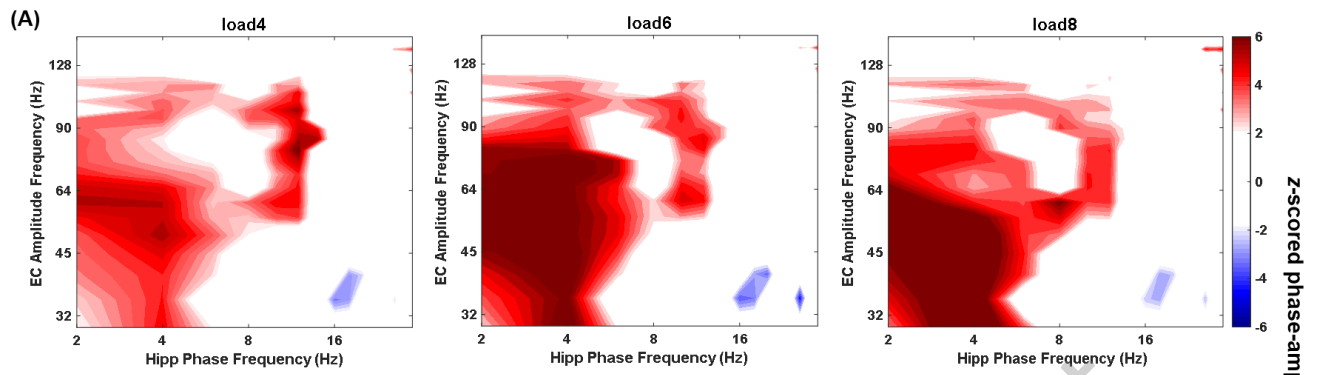


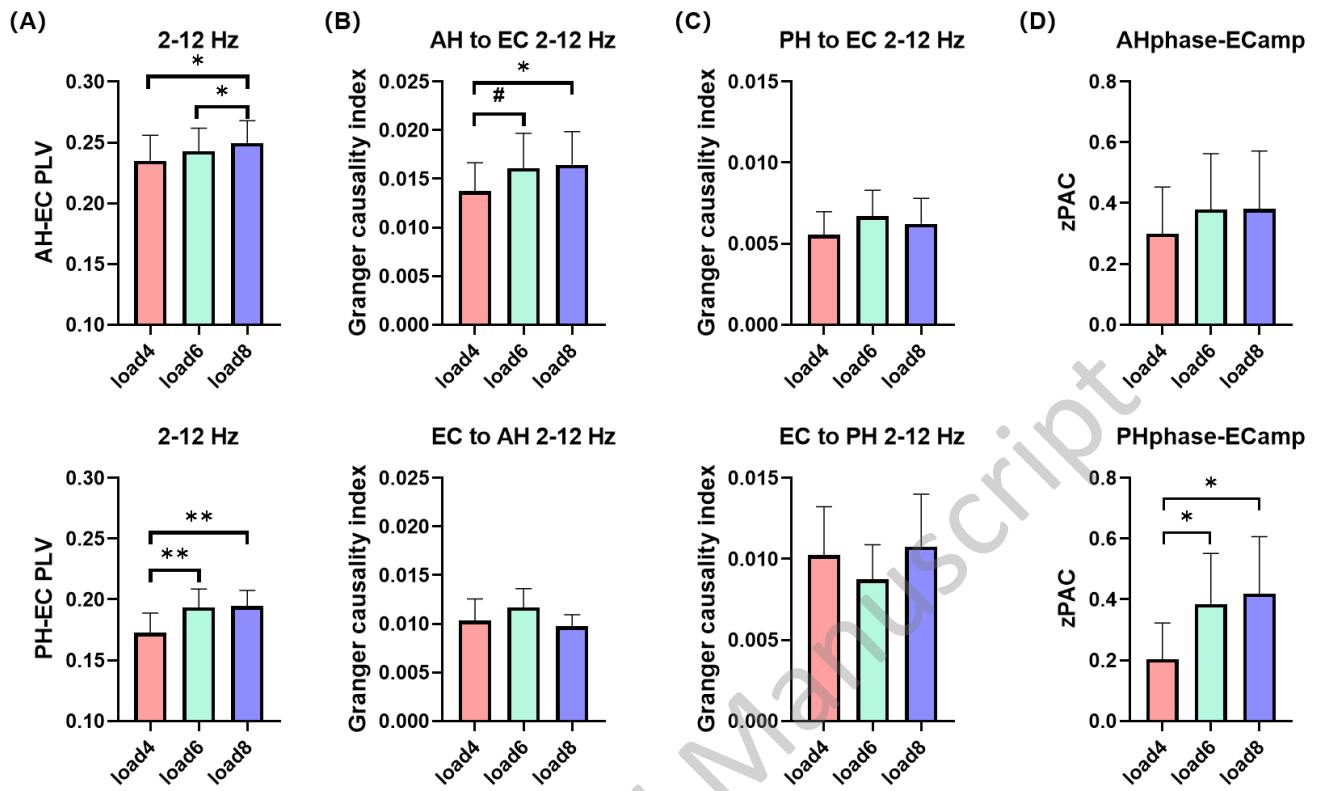
(B)

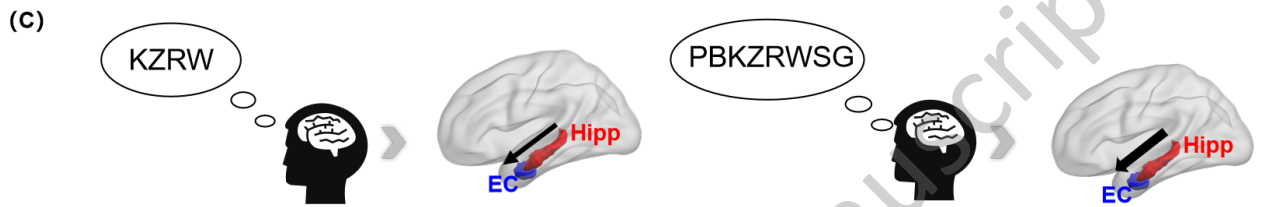
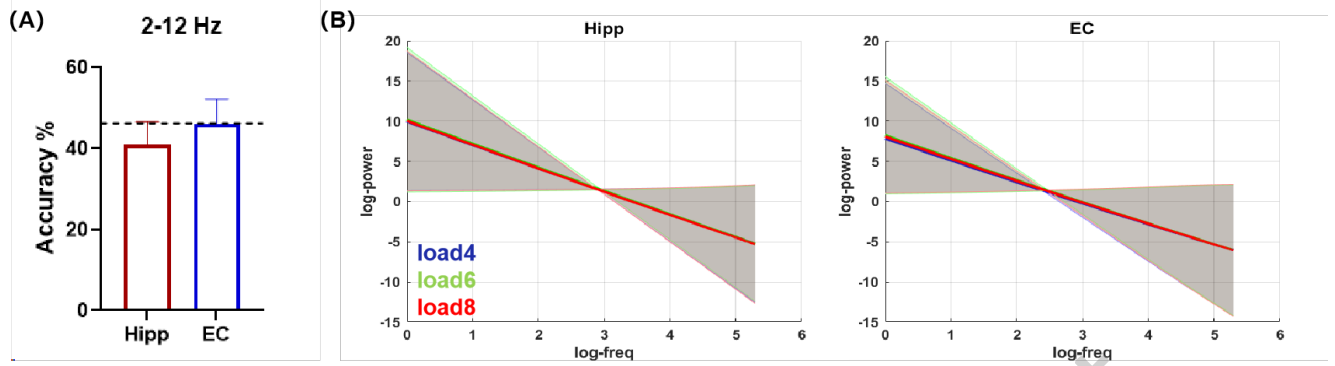


2-12Hz GC









JNeurosci Accepted Manuscript